WHOLE-ROCK AND ND-PB ISOTOPE GEOCHEMISTRY AND RADIOLARIAN AGES OF THE VOLCANICS FROM THE YÜKSEKOVA COMPLEX (MADEN AREA, ELAZIĞ, E TURKEY): IMPLICATIONS FOR A LATE CRETACEOUS (SANTONIAN-CAMPANIAN) BACK-ARC BASIN IN THE SOUTHERN NEOTETHYS

Melek Ural*,✉, **Kaan Sayit**** and **Ugur Kagan Tekin*****

* *Department of Geological Engineering, Fırat University, Elazığ, Turkey.*
** *Department of Geological Engineering, Middle East Technical University, Ankara, Turkey.*
*** *Department of Geological Engineering, Hacettepe University, Ankara, Turkey.*
✉ *Corresponding author, e-mail: melekural@firat.edu.tr*

Keywords: *Yüksekova Complex; Nd-Pb isotopes; subduction; Southern Neotethys; Elazığ; Turkey.*

ABSTRACT

The Southeast Anatolian Orogenic Belt (SAOB) is characterized by a tectonic assemblage consisting of dismembered ophiolites, subduction-related assemblages, and continental fragments. Whether the subduction-related volcanic assemblages formed in a Southern Neotethys oceanic arc-basin system (the Yüksekova Complex) or in a back-arc basin (the Maden Complex) originated after the closure of Southern Neotethys is still debated. To shed light on this matter, we focus on the Maden area, known as the type locality for the Maden Complex. The dating of radiolarian cherts associated with the volcanics from the Maden area yields Late Cretaceous (Santonian-Campanian) ages, indicating that these extrusives belong to the Yüksekova Complex. The Yüksekova volcanics are all subalkaline and mainly characterized by basalts, with subordinate andesitic varieties. The Zr-Nb-Y systematics of the Yüksekova lavas suggest that they have tapped a heterogeneous mantle source region with variable contribution from the depleted mantle. The positive ε_{Nd} values of the volcanics also support the involvement of the depleted mantle. A common feature of the Yüksekova lavas is the marked depletion in Nb relative to Th and La, indicating a subduction-modified mantle source for their petrogenesis. The Pb isotope systematics, particularly the high $^{207}Pb/^{206}Pb$, further implies a variable slab-derived sediment input in the source of these volcanics. Overall, trace element and isotopic characteristics of the Yüksekova lavas are consistent with their generation in an oceanic back-arc basin during the Santonian-Campanian interval in the Southern Neotethys. The Yüksekova back-arc basin characterizes the westward continuum of an extensive Late Cretaceous intra-oceanic subduction system, whose remnants can be traced further to the east, toward Iran.

INTRODUCTION

The majority of the ophiolitic complexes in the eastern Tethyan regions (from Oman to Turkey) obducted onto the Gondwanan-Arabian margin is related to the Late Cretaceous ophiolitic belt (e.g., Moghadam et al., 2009). In the Anatolian sector, the Late Cretaceous ophiolites are traced along the Bitlis-Zagros suture zone, a part of the Southeast Anatolian Orogenic Belt (SAOB). These ophiolites represent remnants of the Southern Neotethys oceanic lithosphere, separating the Tauride-Anatolide Terrane from the Arabian Platform (e.g., Şengör and Yılmaz, 1981; Göncüoglu et al., 1997). In southeast Turkey, around Elazığ and Malatya areas, relics of the Southern Neotethys are preserved within the Amanos-Elazığ-Van Suture Belt, which contains dismembered ophiolitic bodies, arc-related magmatic rocks, and subduction/accretion complexes (Göncüoglu et al., 1997). Within this suture belt, the mélange complexes are dispersed to the north and south of the E-W trending Pütürge and Bitlis metamorphic massifs (e.g., Göncüoglu and Turhan, 1984) (Fig. 1). As a whole, the northerly located mélanges are known as the Yüksekova Complex (Perinçek, 1979).

Several studies suggested that the Southern Neotethys oceanic domain, now preserved in the Amanos-Elazığ-Van Suture Belt, existed between the Late Triassic and Late Cretaceous (Dewey et al., 1973; Perinçek, 1980; Sengör and Yilmaz, 1981; Yazgan, 1981; 1984; Perinçek and Özkaya, 1981; Hempton and Savcı, 1982; Michard et al., 1982; Aktaş and Robertson, 1984). During the Late Cretaceous, the Southern Neotethys oceanic lithosphere became consumed via northward subduction, which also induced the generation of the Yüksekova arc-basin system (Yazgan, 1981; 1984; Ural et al., 2015). The Yüksekova Complex, which holds the relics of this intra-oceanic subduction system, is mainly composed of crustal lithologies with subordinate mantle rocks (Perinçek, 1980; Aktaş and Robertson, 1984; Hempton, 1984; 1985; Kılıç, 2009; Rızaoğlu et al., 2006; 2009; Robertson et al., 2007; Ural and Kürüm, 2009; Tekin et al., 2015; Ural et al., 2015; Yıldırım, 2015; Özdemir, 2016; Rizeli et al., 2016; Uysal et al., 2018; Köküm and İnceöz, 2018, 2020; Sar et al., 2019; Rolland et al., 2020). After the closure of the Southern Neotethys in the Anatolian sector, the region experienced lithospheric extension during the Middle Eocene, which resulted in the opening of a back-arc-type oceanic domain, i.e. the Maden basin (e.g., Sengör and Yilmaz, 1981). The relicts of this small basin are found in the Maden Complex, which is composed of Middle Eocene volcano-sedimentary units (Perinçek, 1979).

The Yüksekova and Maden complexes are, therefore, two distinct identities originated by subduction-related events that took place before and after the closure of Neotethys, respectively. However, the volcanic-bearing nature of both tectonic units has been one of the major challenges in the geology of this area, mostly because without any robust age constraints (geochronological or paleontological), the volcanic-bearing units cropping out along the Elazığ-Amanos-Van Suture Belt have been treated as a part of the Maden Complex. Consequently, a wide range of tectonic settings has been proposed

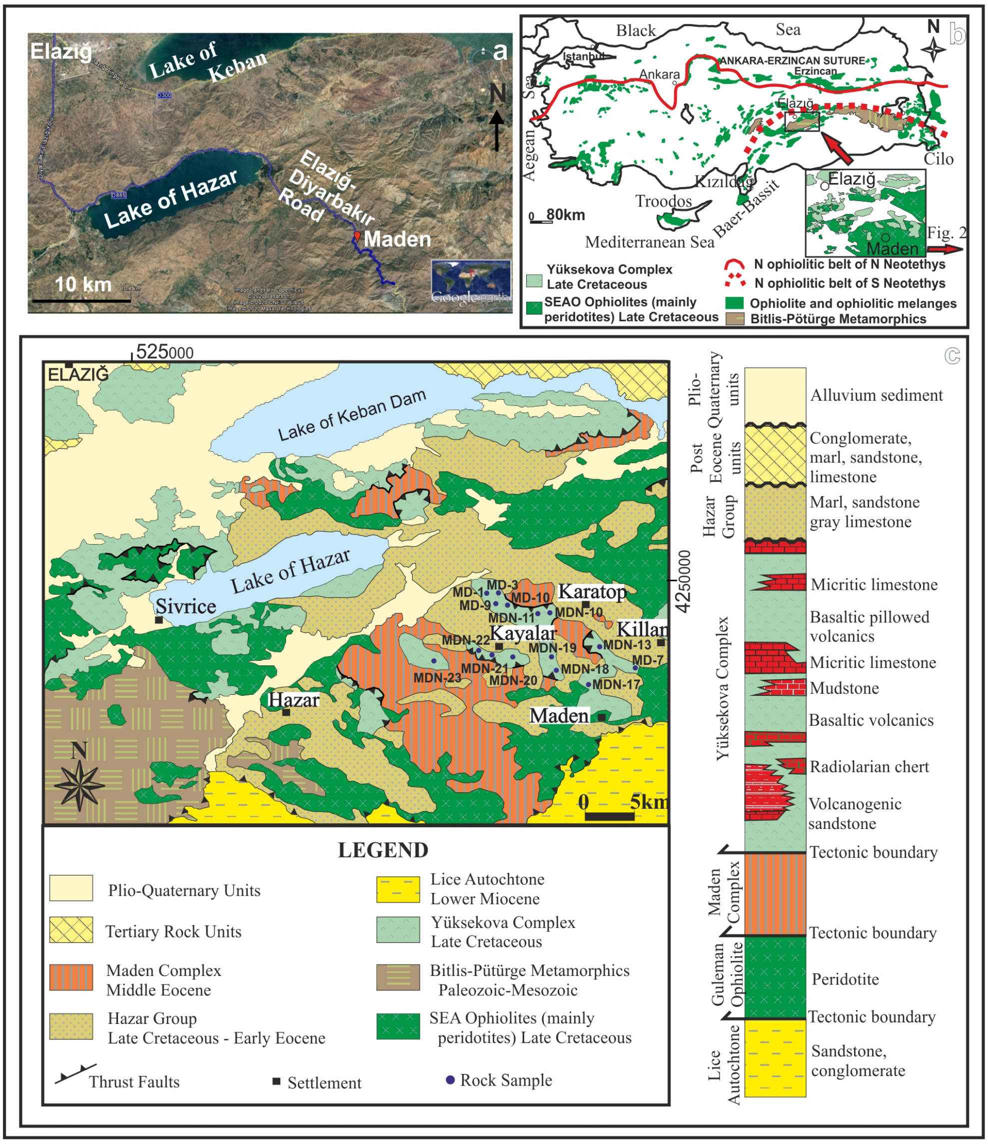

Fig. 1 - a) Google Earth view, b) regional map, and c) simplified geological map with generalized tectonostratigraphic column of the studied area (modified after Tekin et al., 2015; MTA, 2002).

for the origin of the Maden Complex, including mid-ocean ridge, island arc, immature back-arc basin, and continental back-arc basin. The study by Tekin et al. (2015) revealed that a large portion previously considered to belong to the Maden Complex in the previous studies represents, in fact, the Yüksekova Complex. Therefore, the Neotethyan Yüksekova remnants seem to be volumetrically more abundant in the region than previously thought.

Within the SAOB, the age data for the Yüksekova Complex are not abundant. They are mainly paleontology-based, and provide Late Cretaceous ages (e.g., Herece et al., 1992; Robertson et al., 2007; Tekin et al., 2015). However, the age of the volcanics within the complex have been overlooked. In this regard, the studies of Tekin et al. (2015) were the first to perform a detailed characterization, revealing two different age intervals for the Yüksekova volcanism on the basis of the intercalated radiolarian cherts. Another age constraint comes from Ural and Sari (2019), which is based on planktonic foraminiferal fauna from pelagic limestones (Fig. 1c). In this study, we present geochemical (whole-rock and Nd-Pb isotope) and paleontological (radiolarian) data from the Maden area within the SAOB, which were previously dated at Middle Eocene. They were hence considered as part of the Maden Complex. We also aim to integrate the paleontological age constraints with geochemical investigations to solve the Yüksekova-Maden complexes uncertainty. This multidisciplinary approach allowed us to shed light on the Neotethys geodynamics in southeast Anatolia before the closure of the Southern Neotethys.

GEOLOGICAL FRAMEWORK

The SAOB is separated from the northern Tauride-Anatolide Terrane by pre-Maastrichtian south-verging thrusts, which were reactivated during the Late Tertiary. The lowermost tectonic sliver of this terrane contains I-type calc-alkaline plutonic bodies (Baskil Magmatic Arc, Yazgan and Chessex, 1991) of Late Cretaceous age, which were produced by the northward subduction of the southern branch of Neotethys along the southern margin of the Tauride-Anatolide Platform (Malatya-Keban Metamorphics) (Göncüoğlu, 2019). The remnants of the Southern Neotethys Ocean are preserved within a massive mélange complex within the SAOB, consisting of nappes and slide blocks of different origin (oceanic lithosphere, oceanic islands and island arc). The accretion of the oceanic units primarily occurred at the end of the Cretaceous. Afterward, at the end of Miocene the convergence along the suture belt created an imbricated structure in which lithological assemblages of syn- to post-accretional basins were integrated into the suture complex. The SAOB comprises three tectonic zones: i) the Arabian Platform, ii) an imbricated zone, iii) a nappe zone, including fragments of Maden and Yüksekova units. (Yilmaz and Yigitbas, 1991; Yilmaz, 1993).

The Maden Complex (Beken, 1975), first defined as the Maden Series (Ketin, 1948), consists of several distinct lithological assemblages, including a conglomeratic sequence at the bottom (Ceffan Formation); grey-coloured medium-thick-bedded limestones (Arbo Formation); red- to light green-coloured clayey limestones, red marls, red-grey shales, yellow-brown sandstones, siltstones and sandy limestones (Melefan Formation); red marl and limestone alternation (Karadere Formation); sandstone-shale alternation (Narlıdere Formation); basal conglomerates, sandstones and sandy limestones (Maden autochthon deposits), nummulite-bearing limestone blocks, sandstones, volcanic rocks and diabase fragments (olistostromal Maden formation); tuffs, lapillistones, basalts, agglomerates and mudstones (volcanic Maden Formation) (Sungurlu, 1974; Açıkbaş and Baştuğ, 1975; Perinçek, 1979; see also MTA, 2011 for the detailed stratigraphic map). The interpretations on the tectonic setting of the Maden Complex vary, from deep-basin deposits (Rigo de Righi and Cortesini, 1964), mid-ocean ridge (İleri et al., 1976), continental back-arc basin (Perinçek, 1980; Perinçek and Özkaya, 1981; Yazgan, 1981; 1983; 1984; 1987; Özkan, 1983; Yazgan et al., 1983; Michard et al., 1985), immature island arc that developed on a marginal basin (Özkaya, 1978; Erdoğan 1982; Hempton, 1984; 1985; Özçelik, 1985; Yılmaz, 1993; Yılmaz et al., 1993), immature back-arc basin (Perinçek, 1979; Perinçek and Özkaya, 1981; Sengör and Yilmaz, 1981; Erler, 1983;Yigitbas and Yilmaz, 1996).

In the SAOB, the area to the south and southeast of Elazığ contains fragments of both Maden and Yüksekova complexes. The Yüksekova Complex is a typical Late Cretaceous ophiolitic mélange complex and yields widespread outcrops in southeast Anatolia. It consists of a chaotic mixture of basalts, gabbros, serpentinites, pelagic limestones, radiolarian cherts, neritic limestones, granodiorites, sandstones, siltstones, shales with an estimated thickness of about 2000 meters (Perinçek, 1980; 1990; Tekin et al., 2015; Ural and Sarı, 2019; Ural et al., 2021). The age constraints on the Yüksekova Complex come from paleontological findings, which reveal ages between Cenomanian and Maastrichtian. These include: i) Cenomanian-Turonian and Coniacian-Campanian ages from the limestone blocks in the Hakkari area (Perinçek, 1990), ii) Santonian-early Maastrichtian ages from the pelagic limestones based on planktic foraminifera in the Harput area (north of Elazığ) (Herece et al., 1992), iii) late Maastrichtian ages from pelagic limestones within Killan imbricate unit around Maden-Ergani (southeast of Elazığ) (Robertson et al., 2007), iv) Cenomanian-Maastrichtian ages from the pelagic limestones based on radiolarians in the Hazar-Maden area (south-southeast of Elazığ) (Ural et al., 2015), v) late Campanian-late Maastrichtian ages from pelagic limestones based on planktic foraminifera, around Çaybağı (northeast of Elazığ) (Ural and Kaya Sari 2019), vi) Turonian-Santonian ages from the pelagic limestones based on planktonic foraminifera in the Maden town (south of Elazığ) (Ural and Sari, 2019).

To the south/southeast of Elazığ, the Yüksekova Complex crops out widely, being distributed over an area of about 100 km^2 (Fig. 1c). This study involves a wide region including the Karatop, Killan, and Kayalar villages to the North of the Maden town, known as the type locality of the Maden Complex (Fig. 1). To the south of the Hazar Lake (southeast of Elazığ), the volcanics of the Yüksekova Complex are closely associated with and tectonically overlain by mantle rocks of the Guleman Ophiolites. In this area, the Yüksekova volcanics are primarily and widely associated with Cu-mineralizations. Towards the southeast (i.e. near Maden town), the Yüksekova volcanics are unconformably overlain by the Hazar Group, which is made up of non-marine to shallow marine, clastic, and carbonate sedimentary rocks of latest Cretaceous-Early Cenozoic age. In this area, the Yüksekova volcanics are characterized chiefly by basalts in the form of pillowed or massive flows (Fig. S1). The flows are generally gray, green or reddish-coloured and contain abundant gas vesicles. The aphanitic basalts are interbedded with pelagic sediments, including mudstones, micritic limestones (ranging from 10 to 140 cm), radiolarian cherts, and volcaniclastic mudstones, sandstones, and breccias (Fig. 2, Fig. S1).

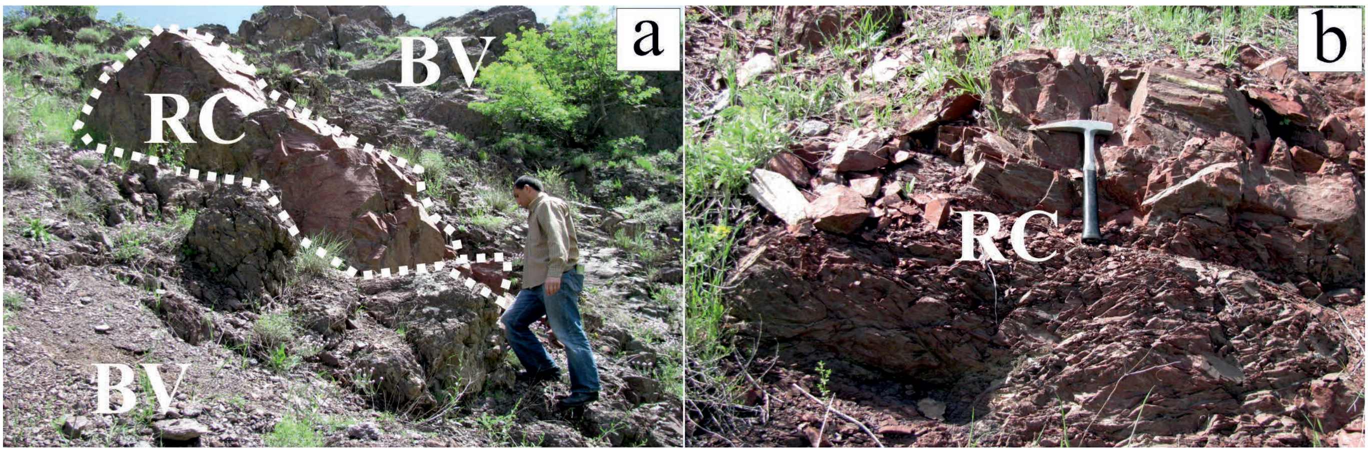

Fig. 2 - Field photographs of the pelagic sedimentary rocks overlying or interlayered with the basalts of the Yüksekova Complex, located in the vicinity of the Maden town (SE Elazığ, Turkey), **a)** Basaltic volcanics (BV) intercalated with meter-thick radiolarian pelagic cherts (RC) and mudstones on the Karatop-Maden road, Sample MDN-18 (x: 561862, y: 4252435), b) Pinkish-coloured, laminated radiolarian pelagic cherts interlayered with the basaltic volcanics, Sample MDN-21 (x:563908, y:4251191).

RADIOLARIAN ASSEMBLAGES FROM THE YÜKSEKOVA COMPLEX AND DATINGS

The radiolarian assemblages have been obtained from six samples (MDN-11, MDN-17, MDN-18, MDN-19, MDN-21 and MDN-22) taken from the Yüksekova Complex (Figs. 3 and 4, Fig. S1) and their ages range from Santonian to Campanian (Late Cretaceous; Fig. 5).

Stratigraphically older specimen derived from the Yüksekova Complex in this study is MDN-11 dominated by Nassellarian fauna (e.g., *Dictyomitra* sp. cf. *D. andersoni* (Campbell and Clark) (Fig. 3.15), *Dictyomitra formosa* Squinabol (Fig. 3.16), *Dictyomitra koslovae* Foreman, *Dictyomitra torquata* Foreman (Fig. 4.3), *Thanarla veneta* (Squinabol) (Fig. 4.8) and *Amphipyndax stocki* (Campbell and Clark) (Fig. 4.9) with exception of *Patellula verteroensis* (Pessagno) (Fig. 5). Within this fauna, *Dictyomitra koslovae* first appears at early Coniacian while LAD of this taxon is at the base of late Maastrichtian according to older literature (e.g., Foreman, 1971; 1975; Nakaseko and Nishimura, 1981; Khokhlova et al., 1994). Besides, recent studies clearly indicate that FAD of this taxon is at the base of Santonian (Korchagin et al., 2012; Bragina et al., 2014; 2019; Bragina, 2016). In addition, this taxon last appears at the top of late Campanian according to Sanfilippo and Riedel (1985). Therefore, it can be concluded that *Dictyomitra koslovae* ranges from Santonian to Campanian (Fig. 5). Another important taxon in this sample is *Dictyomitra torquata* (Fig. 5) and the age range of this taxon is Santonian-Campanian based on the previous studies (e.g., Foreman, 1971; 1973a; 1973b; Yamauchi, 1982; Khokhlova et al., 1994). At last, *Thanarla veneta* is mainly known from Albian-Cenomanian strata (Squinabol, 1903; Nakaseko et al., 1979; Nakaseko and Nishimura, 1981; O'Dogherty, 1994), but according to Soycan and Hakyemez's (2018) this taxon last appears at late Santonian. Based on FAD of *Dictyomitra torquata* and *Dictyomitra koslovae* together with LAD of *Thanarla veneta,* Santonian age can be assigned to sample MDN-11 (Fig. 5).

Other samples (MDN-17, MDN-18, MDN-19, MDN-21 and MDN-22) from the Yüksekova Complex contain similar radiolarian assemblages dominated by Nassellarian taxa (Fig. 5). Sample MDN-17 includes *Dictyomitra formosa* Squinabol (Fig. 3.17), *Dictyomitra koslovae* Foreman (Figs. 3.19-20), *Dictyomitra torquata* Foreman (Fig. 4.4), *Xitus asymbatos* (Foreman) (Fig. 4.10), *Xitus* sp. (Fig. 4.13), *Campanomitra* ? sp. (Fig. 4.14), *Parvimitrella* ? sp. (Fig. 4.15), *Rhopalosyringium* spp. (Figs. 4.19-20), *Clathropyrgus titthium* Riedel and Sanfilippo (Fig. 4.21) and *Afens liriodes* Riedel and Sanfilippo (Fig. 4.22). Similar to this assemblage, *Alievium* spp. (Figs. 3.1-2), *Pseudoaulophacus* sp. (Fig. 3.8), *Patellula verteroensis* (Pessagno) (Fig. 3.12), *Dictyomitra formosa* Squinabol, *Dictyomitra koslovae* Foreman, *Dictyomitra torquata* Foreman, *Xitus asymbatos* (Foreman) (Fig. 4.11), *Rhopalosyringium* sp. cf. *R. colpodes* Foreman (Fig. 4.18) were determined from sample MDN-18 (Fig. 5).

The sample MDN-19 contains very-diverse assemblage: *Alievium* spp., *Pseudoaulophacus lenticulatus* (White) (Fig. 3.4), *Pseudoaulophacus pargueraensis* Pessagno (Fig. 3.6), *Pseudoaulophacus* sp. (Fig. 3.9), *Archaeospongoprunum nishiyamae* Nakaseko and Nishimura (Fig. 3.11), *Patellula verteroensis* (Pessagno) (Fig. 3.13), *Dictyomitra formosa* Squinabol (Fig. 3.18), *Dictyomitra koslovae* Foreman (Fig. 3.21), *Dictyomitra torquata* Foreman (Fig. 4.5), *Xitus asymbatos* (Foreman) (Fig. 4.12), *Parvimitrella* sp. and *Dictyoprora urna* (Foreman) (Fig. 4.17). The radiolarian assemblage of the sample MDN-21 contains *Alievium* spp., *Pseudoaulophacus lenticulatus* (White), *Pseudoaulophacus* sp. cf. *P. pargueraensis* Pessagno (Fig. 3.7), *Pseudoaulophacus* sp. (Fig. 3.10), *Crucella* spp., *Homoeparonaella* spp., *Patellula* sp. cf. *P. verteroensis* (Pessagno) (Fig. 3.14), *Dictyomitra formosa* Squinabol, *Dictyomitra koslovae* Foreman (Fig. 3.22), *Dictyomitra* sp. cf. *D. napaensis* Pessagno (Fig. 4.2), *Dictyomitra torquata* Foreman, *Mita* sp. (Fig. 4.7), *Afens liriodes* Riedel and Sanfilippo (Fig. 4.23). In addition, less-diverse radiolarians were obtained from sample MDN-22 (e.g., *Alievium* sp. at fig. 3.3, *Pseudoaulophacus lenticulatus* (White) at fig. 3.5, *Pseudoaulophacus* sp., *Dictyomitra koslovae* Foreman at fig. 3.23, *Dictyomitra multicostata* Zittel at fig. 4.1, *Dictyomitra* sp. at fig. 4.6 and *Parvimitrella* ? sp. at fig. 4.16; fig. 5).

Although all these samples (MDN-17, MDN-18, MDN-19, MDN-21 and MDN-22) contain mainly long-ranging taxa (e.g., *Patellula verteroensis, Pseudoaulophacus lenticulatus, Pseudoaulophacus pargueraensis, Dictyomitra formosa*, *Xitus asymbatos* and *Afens lirioides*; Fig. 5), they include also two well-known and stratigraphically important taxa (*Dictyomitra koslovae* and *Dictyomitra torquata*) except for the sample MDN-22 (including only *Dictyomitra koslovae*; Fig. 5). Ranges of these taxa is from Santonian to Campanian according to previous studies (e.g., Foreman, 1971; 1973a; 1973b; Yamauchi, 1982; Sanfilippo and Riedel, 1985; Khokhlova et al., 1994; Korchagin et al., 2012; Bragina et al., 2014; 2019; Bragina, 2016).

In addition, *Clathropyrgus titthium* in sample MDN-17 last appears at the top of late Campanian according to Riedel and Sanfilippo (1974), Foreman (1975), Sanfilippo and Riedel (1985). The presence of this taxon in sample MDN-17 also clearly defines the upper age limit of this sample as top of late Campanian (Fig. 5). Diverse fauna obtained from sample MDN-19 includes also two well-known taxa, *Archaeospongoprunum nishiyamae and Dictyoprora urna,* that have their last appearance at the top of late Campanian (Foreman, 1971; Riedel and Sanfilippo, 1974; Nakaseko and Nishimura, 1981; Sanfilippo and Riedel, 1985). Thus the presence of these two taxa, in addition to the presence of *Dictyomitra koslovae* and *Dictyomitra torquata* (Fig. 5), define the upper age limit of the sample MDN-19, as top of late Campanian. Based on these facts, it can be concluded that Santonian to Campanian age can be assigned to samples MDN-17, MDN-18, MDN-19, MDN-21 and MDN-22 obtained from the Yüksekova Complex (Fig. 5).

PETROGRAPHY

The majority of volcanic rocks cropping out around the Maden area (SE of Elazığ) are porphyritic with variable amounts of phenocrysts set in a finely crystallized matrix. The dominant phenocryst phases are clinopyroxene and plagioclase (Fig. 6a-f). Rare olivine-phyric varieties are observed in the basaltic types, while minor K-feldspar is found in the evolved compositions. Hyalopilitic lavas consisting of small plagioclase microlites embedded in altered glass matrix are common (Figs. 6a-b). Intersertal texture is also frequent (Fig. 6e). Coarse-grained samples are generally aphyric, holocrystalline, while porphyritic texture becomes dominant in the fine-grained samples with a glassy matrix (Fig. 6a-d). Gas vesicles and fractures are filled by secondary phases such as calcite or quartz (Fig. 6). The most abundant primary mafic mineral is clinopyroxene, which largely occurs as phenocryst, whereas it is less abundant as ground-

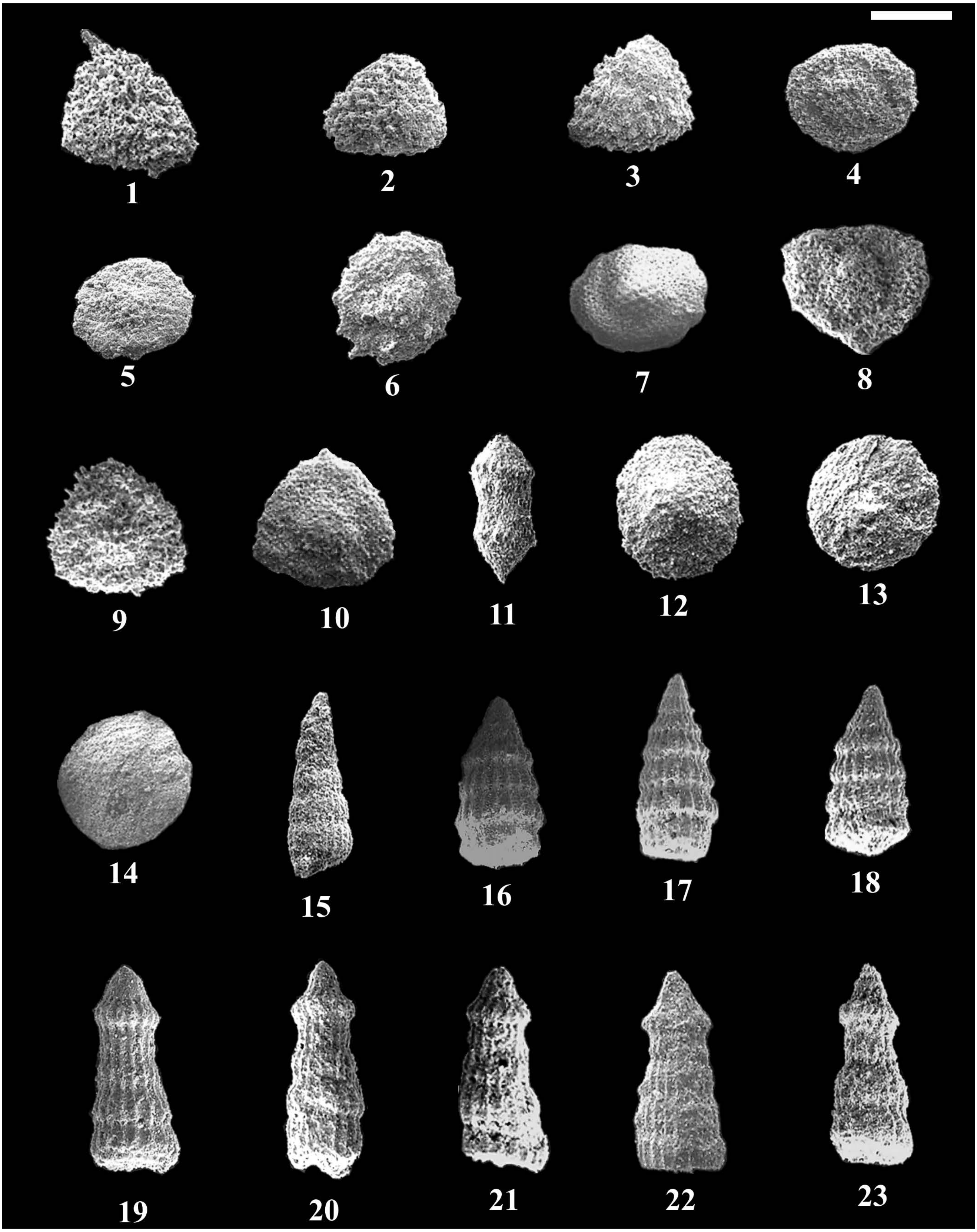

Fig. 3 - Scanning electron photomicrographs of the Late Cretaceous (Santonian-Campanian) radiolarians from the Yüksekova Complex, eastern and southeastern Turkey. Scale- number of microns for each figure: 1-3. *Alievium* spp., 1-2. MDN-18, 3. MDN-22, scale bar- 120µm for all figures; 4-5. *Pseudoaulophacus lenticulatus* (White), 4. MDN-19, 5. MDN-22, scale bar- 160 and 140µm, respectively; 6. *Pseudoaulophacus pargueraensis* Pessagno, MDN-19, scale bar- 120µm; 7. *Pseudoaulophacus* sp. cf. *P. pargueraensis* Pessagno, MDN-21, scale bar- 120µm; 8-10. *Pseudoaulophacus* spp., 8. MDN-18, 9. MDN-19, 10. MDN-21, scale bar- 120, 120 and 110µm, respectively; 11. *Archaeospongoprunum nishiyamae* Nakaseko and Nishimura, MDN-19, scale bar- 110µm; 12-13. *Patellula verteroensis* (Pessagno), 12. MDN-18, 13. MDN-19, scale bar- 160 and 170 µm, respectively; 14. *Patellula* sp. cf. *P. verteroensis* (Pessagno), MDN-21, scale bar-140µm; 15. *Dictyomitra* sp. cf. *D. andersoni* (Campbell and Clark), MDN-11, scale bar- 110µm; 16-18. *Dictyomitra formosa* Squinabol, 16. MDN-11, 17. MDN-17, 18. MDN-19, scale bar- 100, 100 and 120µm, respectively; 19-23. *Dictyomitra koslovae* Foreman, 19-20. MDN-17, 21. MDN-19, 22. MDN-21, 23. MDN-22, scale bar- 90, 100, 100, 90 and 100µm, respectively.

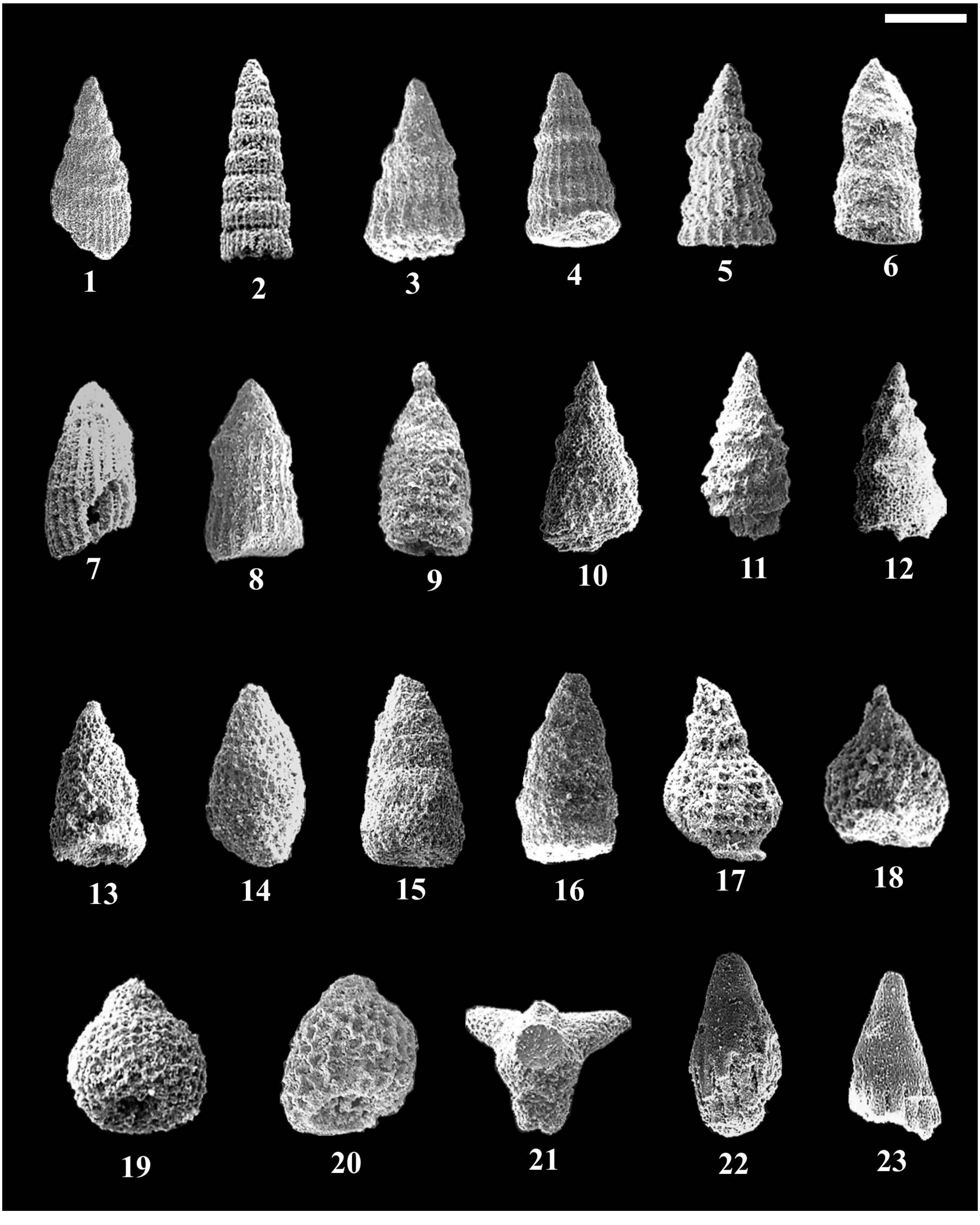

Fig. 4 - Scanning electron photomicrographs of the Late Cretaceous (Santonian-Campanian) radiolarians from the Yüksekova Complex, eastern and southeastern Turkey. Scale- number of microns for each figure: 1. *Dictyomitra multicostata* Zittel, MDN-22, scale bar- 100µm; 2. *Dictyomitra* sp. cf. *D. napaensis* Pessagno, MDN-21, scale bar- 90µm; 3-5. *Dictyomitra torquata* Foreman, 3. MDN-11, 4. MDN-17, 5. MDN-19, scale bar- 80, 90 and 100µm, respectively; 6. *Dictyomitra* sp., MDN-22, scale bar- 80µm; 7. *Mita* sp., MDN-21, scale bar- 90µm; 8. *Thanarla veneta* (Squinabol), MDN-11, scale bar- 65µm; 9. *Amphipyndax stocki* (Campbell and Clark), MDN-11, scale bar- 60µm; 10-12. *Xitus asymbatos* (Foreman), 10. MDN-17, 11. MDN-18, 12. MDN-19, scale bar- 130, 100 and 130µm, respectively; 13. *Xitus* sp., MDN-17, scale bar- 110µm; 14. *Campanomitra* ? sp., MDN-17, scale bar- 80µm; 15-16. *Parvimitrella* ? spp., 15. MDN-17, 16. MDN-22, scale bar- 80 and 90µm, respectively; 17. *Dictyoprora urna* (Foreman), MDN-19, scale bar- 70µm; 18. *Rhopalosyringium* sp. cf. *R. colpodes* Foreman, MDN-18, scale bar- 90µm; 19-20. *Rhopalosyringium* spp., both from MDN-17, scale bar- 60µm for both specimens; 21. *Clathropyrgus titthium* Riedel and Sanflippo, MDN-17, scale bar- 100µm; 22-23. *Afens liriodes* Riedel and Sanfilippo, 22. MDN-17, 23. MDN-21, scale bar- 100µm for both specimens.

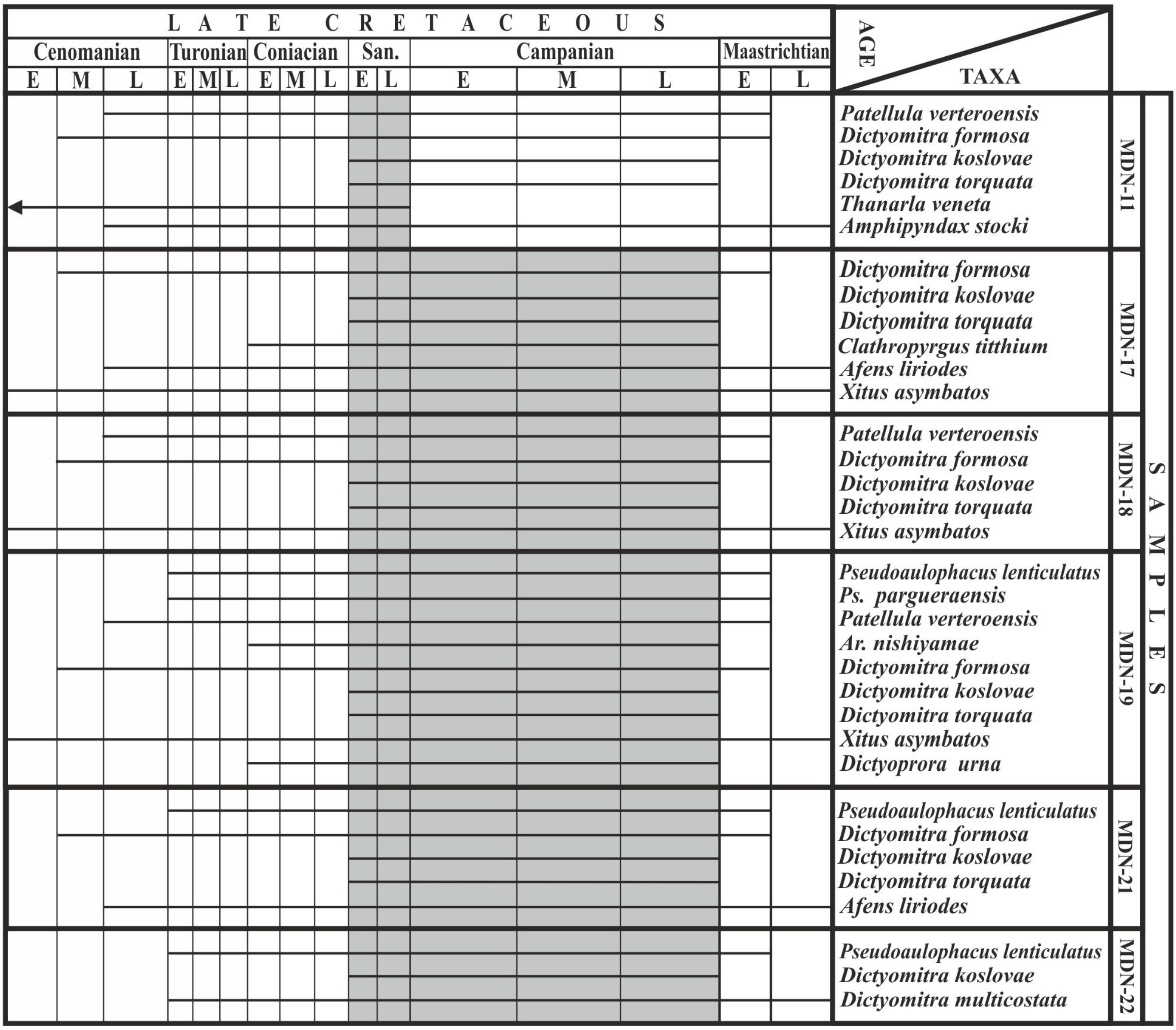

Fig. 5 - Distribution of radiolarian taxa from samples of the Yüksekova Complex. Grey areas show the ages of radiolarian assemblages.

mass phase. Zoning and twinning are common on clinopyroxene. Olivine is rarely observed as a relict mineral due to intense alteration. Plagioclase is very abundant both as a phenocryst and groundmass phase. Polysynthetic twinning is recognizable in the less altered crystals. Glomeroporphyritic clusters composed of plagioclase and clinopyroxene are found in some samples (Fig. 6e). Mafic minerals may be entirely pseudomorphosed by secondary minerals. Chlorite and epidote are typical alteration products in the lavas, replacing clinopyroxenes and/or the glassy groundmass. Plagioclase may be partly albitized and sericitized or, in some cases, replaced by zeolites.

GEOCHEMISTRY

Analytical methods

A total of 16 samples were selected for whole-rock geochemistry. Eight samples previously presented in Ural et al. (2015) were reanalyzed specifically for this paper. The whole-rock geochemical analyses were performed at the Activation Labs (Canada) (Table 1). For the analyses of major oxides and some trace elements (i.e. Sc, V, Ba, Sr, and Zr), the samples were fluxed with lithium metaborate/tetraborate and later digested with 5% nitric acid. These elements were analyzed by inductively coupled plasma-optical emission spectrometry (ICP-OES). Other trace elements (except for Pb and Ni) were similarly prepared by lithium metaborate/tetraborate fusion. They were analyzed by inductively coupled plasma-mass spectrometry (ICP-MS). Pb and Ni were analyzed by ICP-MS after digestion with four acids (hydrochloric, hydrofluoric, nitric, and perchloric acids).

Nd and Pb isotopic compositions of the Yüksekova volcanics were measured on a total of ten selected samples by Nu Instruments Plasma MC-ICP-MS (multi-collector inductively coupled plasma mass spectrometry) at the Pacific Centre for Isotopic and Geochemical Research (PCIGR) at the University of British Columbia (Canada) (Table 2). The JNdi

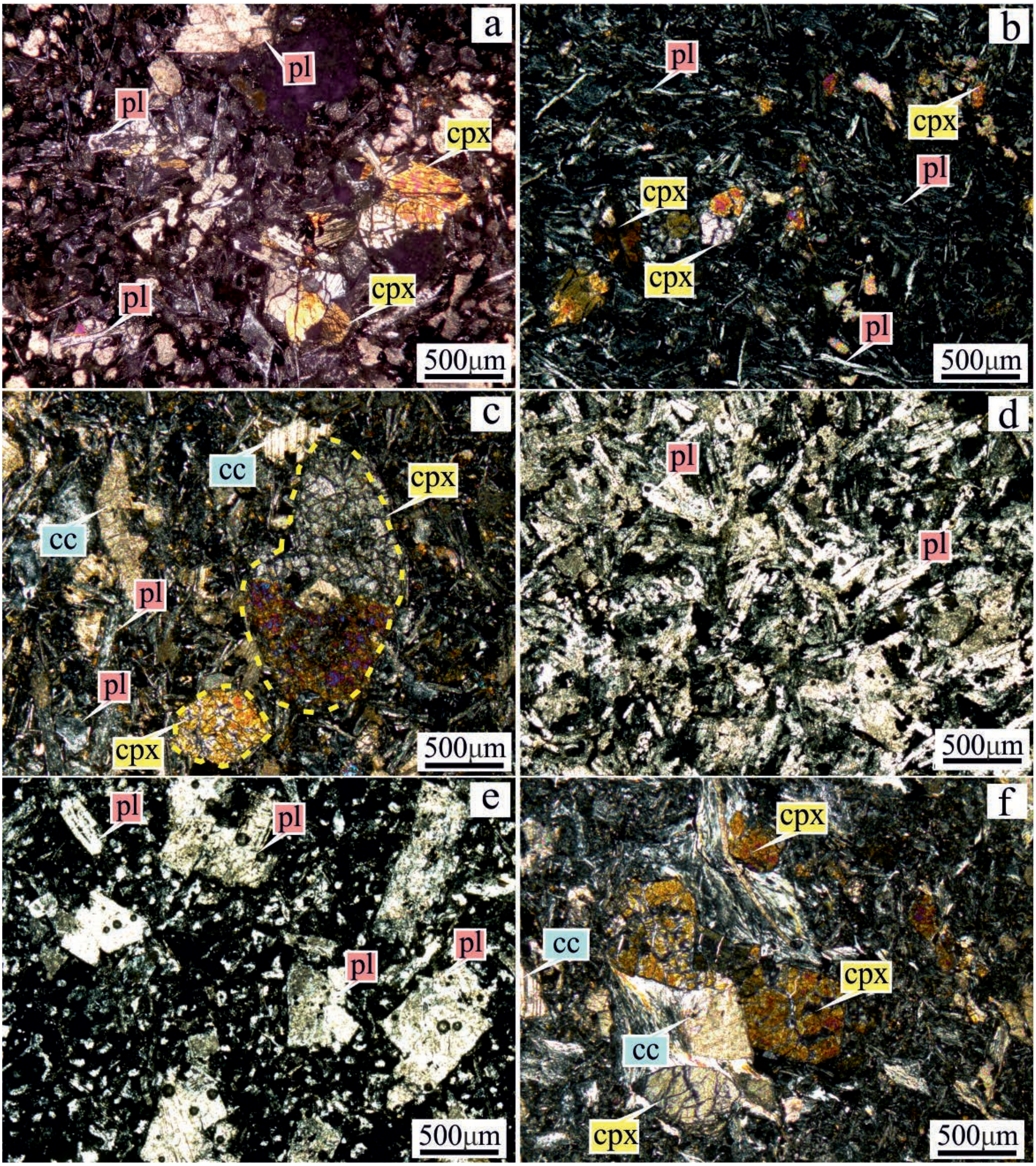

Fig. 6 - Microphotographs of the volcanics from the Yüksekova Complex around the Maden town: **a)** Hyalomicrolithic basalt (MD-1), **b)** Porphyritic basalt with flow texture (MD-3), **c)** Hyalomicrolitic porphyritic basalt (MDN-11), **d)** Aphyric basalt (MDN-17), **e)** Hyalomicrolitic porphyritic basalt (MDN-19), **f)** Clinopyroxene-phyric basalt (MDN-21). Abbreviations: pl- plagioclase, cpx- clinopyroxene, op- opaque oxide, cc- calcite.

standard gave a mean $^{143}Nd/^{144}Nd$ = 0.512077±0.000007 (2sd, n = 27). NBS 981 Pb standard gave a mean (n = 15) $^{208}Pb/^{204}Pb$ = 36.7219±0.0021 (2sd), $^{207}Pb/^{204}Pb$ = 15.4994±0.0008 (2sd), and $^{206}Pb/^{204}Pb$ = 16.9432 ± 0.0009 (2sd). The Nd isotope values are normalized to $^{143}Nd/^{144}Nd$ = 0.512116 for JNdi, whereas the Pb values are normalized to $^{208}Pb/^{204}Pb$ = 36.7219 for, $^{207}Pb/^{204}Pb$ = 15.4963 and $^{206}Pb/^{204}Pb$ = 16.9405 for the triple spike values of Galer and Abouchami (1998).

Table 1 - Whole rock major wt.(%) and trace element (ppm) composition of the studied rocks.

Sample name	MD-1	MD-2	MD-3	MD-7	MD-9	MD-10	MDN-10	MDN-11	MDN-13	MDN-17	MDN-18	MDN-19	MDN-20	MDN-21	MDN-22	MDN-23
SiO_2	48.40	45.09	44.75	45.21	47.83	49.75	73.31	44.45	49.24	49.16	49.18	46.05	64.84	45.44	65.43	66.21
Al_2O_3	12.41	16.42	13.78	15.76	15.35	16.62	10.14	15.18	18.54	13.62	15.99	14.28	14.71	15.61	8.29	15.88
$Fe_2O_{3(T)}$	7.39	9.88	8.57	8.21	12.46	8.82	6.93	8.55	8.89	7.50	8.34	7.55	3.97	8.73	4.22	5.30
MnO	0.10	0.14	0.14	0.09	0.11	0.10	0.09	0.14	0.18	0.35	0.17	0.29	0.03	0.18	1.18	0.10
MgO	11.98	6.82	7.66	2.63	7.53	2.73	1.24	5.50	5.40	3.60	3.53	4.53	0.06	5.01	5.76	0.68
CaO	6.72	9.24	10.49	12.66	6.34	9.52	1.13	12.87	6.38	10.45	7.70	11.68	4.39	10.21	6.28	1.18
Na_2O	1.22	3.59	4.24	3.17	2.92	3.41	4.93	3.53	5.46	5.68	6.36	3.04	8.62	2.29	0.61	9.19
K_2O	0.35	0.68	0.85	0.73	0.24	0.50	0.07	0.85	0.24	0.11	0.43	1.33	0.02	1.97	0.43	0.03
TiO_2	0.557	0.810	0.828	0.802	1.682	0.917	0.948	0.860	1.018	0.775	0.865	0.766	0.624	1.038	0.457	0.775
P_2O_5	0.03	0.09	0.11	0.15	0.17	0.17	0.21	0.17	0.25	0.13	0.16	0.14	0.23	0.16	0.14	0.27
LOI	10.14	7.00	8.78	9.90	5.51	8.07	1.10	7.70	4.95	7.89	6.40	9.83	2.44	7.91	6.50	0.76
Total	99.32	99.79	100.20	99.32	100.10	100.60	100.10	99.79	100.60	99.26	99.13	99.49	99.94	98.54	99.31	100.40
Sc	29	38	35	25	33	26	14	28	23	23	29	23	7	30	13	16
V	222	278	235	553	401	781	49	264	202	213	338	134	96	281	170	96
Rb	9.2	8.1	11.8	10.7	2.8	7	0.7	10.3	3.2	1.7	4.7	24.5	0.2	25.6	15.1	0.1
Sr	125	214	344	362	170	365	65	431	678	387	354	321	53	263	82	174
Y	13.4	18.4	20.9	18.7	40.5	20.6	46.7	18.9	23	16.8	19.3	19.3	40.9	21.8	21.4	65.6
Zr	42	41	50	70	106	76	115	84	99	61	81	65	203	73	74	292
Nb	4.3	1.5	1.6	2.8	2.7	2.9	1.8	1.6	4.7	3.3	1.4	1.6	7.3	3.3	6.7	4.2
Ba	36	51	127	58	16	52	24	102	53	55	79	103	11	165	69	34
Hf	1.0	1.3	1.4	1.7	2.8	1.9	3.0	1.8	2.3	1.5	1.9	1.6	4.6	1.9	1.8	6.8
Ta	0.34	0.10	0.11	0.26	0.21	0.25	0.15	0.14	0.39	0.28	0.11	0.15	0.65	0.27	0.58	0.35
Th	1.05	0.50	0.42	0.79	0.44	0.84	0.41	0.97	1.15	0.62	0.94	0.91	3.06	1.16	4.44	4.10
Pb	4.2	1.0	2.2	1.8	1.1	2.0	1.3	1.4	1.8	5.0	6.8	6.9	5.3	2.5	2.8	3.4
La	7.22	5.10	3.76	7.13	5.23	7.47	5.77	8.73	9.87	6.13	8.11	8.17	21.40	9.82	14.40	26.90
Ce	11.70	8.70	8.59	15.80	13.70	16.60	16.30	19.70	23.10	13.20	17.50	17.30	45.20	21.40	27.40	58.00
Pr	1.70	1.31	1.33	2.13	2.17	2.32	2.61	2.68	3.09	1.91	2.35	2.43	5.77	2.98	4.43	8.72
Nd	7.10	6.10	6.60	9.70	11.40	10.70	13.90	11.50	14.60	8.70	10.70	11.00	23.70	13.40	18.20	37.50
Sm	1.75	1.76	2.04	2.69	3.72	2.87	4.53	2.96	3.41	2.32	2.65	2.71	5.46	3.47	4.28	9.57
Eu	0.58	0.72	0.79	0.94	1.46	1.07	1.40	1.01	1.24	0.84	0.98	0.99	1.56	1.17	0.86	2.52
Gd	2.10	2.56	2.94	2.96	5.29	3.41	6.40	3.20	3.83	2.69	3.08	2.99	5.69	3.62	3.82	10.60
Tb	0.38	0.47	0.54	0.52	1.01	0.61	1.22	0.55	0.65	0.47	0.56	0.55	0.96	0.63	0.63	1.84
Dy	2.30	3.02	3.46	3.16	6.57	3.69	7.72	3.40	4.03	2.86	3.39	3.34	6.26	3.82	3.62	11.50
Ho	0.46	0.67	0.72	0.66	1.41	0.74	1.62	0.67	0.81	0.58	0.67	0.67	1.29	0.78	0.69	2.31
Er	1.33	2.00	2.07	1.98	4.20	2.21	4.83	1.93	2.38	1.67	1.94	1.96	3.99	2.23	2.00	6.79
Tm	0.19	0.28	0.31	0.30	0.63	0.32	0.72	0.28	0.35	0.24	0.29	0.28	0.63	0.33	0.31	1.01
Yb	1.29	1.76	2.06	1.90	4.28	2.14	4.83	1.82	2.26	1.64	1.93	1.82	4.31	2.16	2.10	7.13
Lu	0.20	0.27	0.34	0.31	0.69	0.34	0.78	0.29	0.36	0.26	0.31	0.28	0.73	0.33	0.31	1.16

$Fe_2O_{3(T)}$ is total Fe expressed as Fe^{3+}. LOI: Loss on ignition.

Table 2 - Whole-rock Nd and Pb isotopic compositions of the studied rocks.

Sample	MD-1	MD-3	MD-7	MD-9	MD-10	MDN- 11	MDN- 13	MDN- 17	MDN- 19	MDN- 21
Sm	1.75	2.04	2.69	3.72	2.87	2.96	3.41	2.32	2.71	3.47
Nd	7.14	6.56	9.73	11.40	10.70	11.50	14.60	8.70	11.00	13.40
$^{143}Nd/^{147}Sm$	0.1488	0.1888	0.1678	0.1981	0.1628	0.1562	0.1418	0.1619	0.1495	0.1572
$^{143}Nd/^{144}Nd$	0.512714	0.512921	-	0.512979	0.512973	0.512944	0.512941	0.512943	0.512929	0.512930
2SE	0.000007	0.000007	-	0.000006	0.000007	0.000007	0.000007	0.000007	0.000006	0.000006
$^{143}Nd/^{144}Nd_{(i)}$	0.512636	0.512823	-	0.512876	0.512888	0.512863	0.512867	0.512859	0.512850	0.512852
$\varepsilon_{Nd(i)}$	+2.0	+5.6	-	+6.7	+6.9	+6.4	+6.5	+6.3	+6.2	+6.1
U	0.32	0.13	0.20	0.32	0.24	0.27	0.39	0.30	0.20	0.15
Th	1.05	0.42	0.79	0.44	0.84	0.97	1.15	0.62	0.91	1.16
Pb	4.2	2.2	1.8	1.1	2.0	1.4	1.8	5.0	6.9	2.5
$^{206}Pb/^{204}Pb$	18.9313	18.632	18.7345	18.6598	18.7477	19.0824	18.7295	18.7983	18.7869	18.8926
2SE	0.00003	0.00004	0.00004	0.00004	0.00003	0.00004	0.00003	0.00004	0.00004	0.00003
$^{206}Pb/^{204}Pb_{(i)}$	18.8726	18.5864	18.6489	18.4356	18.6552	18.9337	18.5625	18.7521	18.7416	18.8703
$^{207}Pb/^{204}Pb$	15.6728	15.5924	15.566	15.5151	15.5458	15.5831	15.5475	15.6458	15.6344	15.5971
2SE	0.00001	0.00001	0.00001	0.00001	0.00001	0.00001	0.00001	0.00001	0.00001	0.00001
$^{207}Pb/^{204}Pb_{(i)}$	15.6698	15.5901	15.5617	15.5038	15.5411	15.5756	15.5395	15.6434	15.6333	15.5948
$^{208}Pb/^{204}Pb$	39.01666	38,5989	38,5069	38,4183	38,4968	38,8312	38,4544	38,8087	38,7967	38,7875
2SE	0.000002	0.000003	0.000002	0.000002	0.000002	0.000002	0.000002	0.000002	0.000002	0.000002
$^{208}Pb/^{204}Pb_{(i)}$	38.9533	38.5506	38.3959	38.3172	38.3906	38.6559	38.2928	38.7773	38.7618	38.7542

Initial Nd and Pb isotopic ratios are calculated back to t = 80 Ma based on the radiolarian ages obtained in this study.
ε_{Nd} values were computed as the deviation from a chondritic uniform reservoir (CHUR) with present-day $^{143}Nd/^{144}Nd$ = 0.512638; $^{147}Sm/^{144}Nd$ = 0.1966.

Results

Based on immobile element ratios, the Yüksekova volcanics in the Maden region are mainly classified as basalts, though subordinate basaltic/andesitic compositions also occur (Fig. 7a). We avoid using the classification schemes like TAS and AFM due to the altered nature of the studied volcanics (see Discussion). All samples have relatively low Nb/Y (0.04-0.32), indicating their sub-alkaline character, and display transitional features between calc-alkaline and tholeiitic (Fig. 7b). The samples show a large variation in SiO_2 content from 44.45 to 73.31 wt%, which may partly result from alteration and/or magmatic modification processes. CaO, Fe_2O_3, and MgO also display broad ranges between 1.13-12.87 wt%, 3.97-12.46 wt% and 0.06-11.98 wt%, respectively. Trace elements exhibit large compositional variation (e.g., V = 49-781 ppm, Cr = 7-193 ppm, Ni = 2.1-133 ppm, Rb = 0.1-25.6 ppm, Sr = 53-678 ppm, Zr = 42-292 ppm, see Table 1).

In multi-element plots normalized to N-MORB (Fig. 8a), the Yüksekova volcanics are all characterized by variable enrichments in Th and La relative to Nb, exhibiting strong Nb negative anomalies (Nb/Nb* = 0.09-0.42). Also, most samples display relative enrichment in large ion lithophile elements (LILE) (i.e. Rb, Ba, K, Sr) and LREE (with an increasing magnitude towards La) relative to high field-strength elements (HFSE). Although the investigated rocks exhibit broadly similar characteristics, two main patterns emerge on the basis of fluid-immobile trace element systematics compared to N-MORB. One type, represented by only two samples in the dataset (MD-9 and MDN-10, Type 1), is characterized by relatively flat distribution of REE and HFSE (except for Nb and Ti). The other type (Type 2) is LREE-enriched and possesses higher Th concentrations

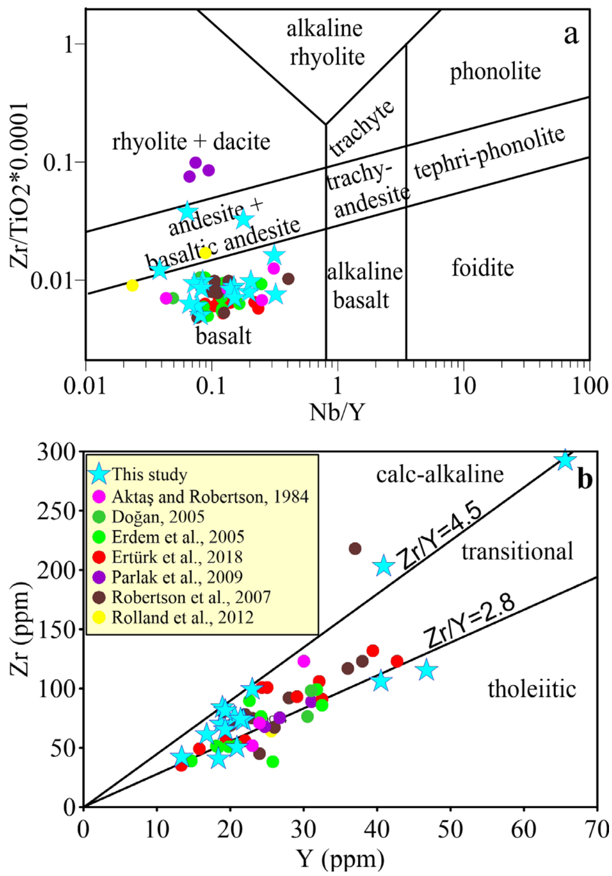

Fig. 7 - Chemical classification of the Yüksekova volcanics according to a) Nb/Y vs. Zr/TiO_2 diagram of Winchester and Floyd (1977) revised after Pearce (1996); b) Zr vs. Y diagram (Barrett and MacLean, 1997) revised after Ross and Bedard (2009).

(with respect to Nb). While the Nb concentrations in the first type are similar to N-MORB, the second type displays highly variable Nb contents, generally more enriched than N-MORB. All samples possess negative Ti anomalies; however, this depletion is particularly significant for silica-rich samples. In chondrite-normalized diagrams (Fig. 8b), the samples display LREE-depleted (Type 1) to flat- to LREE-enriched (shown by the Type 2) patterns. HREE appear to be relatively flat in all samples. Negative Eu anomaly is noticeable only in a few samples (Eu/Eu* = 0.65-1.07, with an average of 0.96).

The Nd and Pb isotopic ratios of the Yüksekova volcanics from the Maden area (SE Elazığ) are presented in Table 2. All isotopic values were corrected to 80 Ma in agreement with the radiolarian ages obtained in this study. As a whole, the analyzed samples display a moderate variability of initial Nd isotope composition ($^{143}Nd/^{144}Nd_{(i)}$ = 0.51271-0.51298). Most $\varepsilon_{Nd(i)}$ values range between +5.6 and +6.9 excepting the sample MD-1, which has an $\varepsilon Nd_{(i)}$ of +2.0 (Fig. 9a). In terms of Pb isotopic compositions, the studied rocks show moderately variable Pb isotope compositions ($^{206}Pb/^{204}Pb$ =18.44-18.93, $^{208}Pb/^{204}Pb$ = 38.29-38.95). $^{207}Pb/^{204}Pb$ ratios, on the other hand, display more variability with values ranging between 15.50-15.67. The $^{207}Pb/^{204}Pb$ and $^{208}Pb/^{204}Pb$ ratios show broad positive correlations with $^{206}Pb/^{204}Pb$ (Figs. 9b-c). Remarkably, $^{207}Pb/^{204}Pb$ values are significantly displaced from the MORB field towards EM-II and GLOSS (global subducting sediment) compositions (Fig. 9b). The distributions of the volcanics in this study appear to be similar to the group 2 samples of Ural et al. (2015), who reported the first isotopic data in this area (Fig. 9).

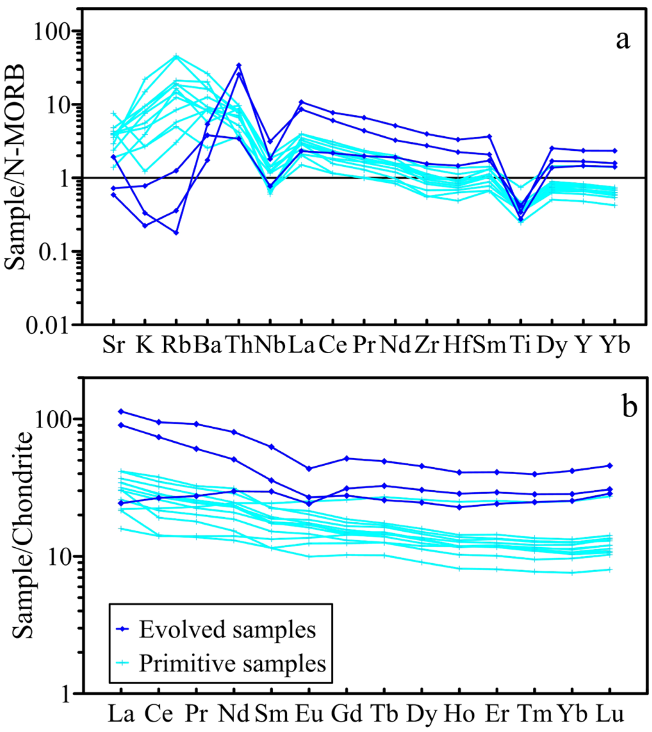

Fig. 8 - a) Multi-element and b) REE patterns for the studied samples normalized to N-MORB and chondrite, respectively (normalization values are from Sun and McDonough, 1989). The primitive samples are indicated by light blue cross symbol, whereas the evolved ones are represented by blue diamond symbol.

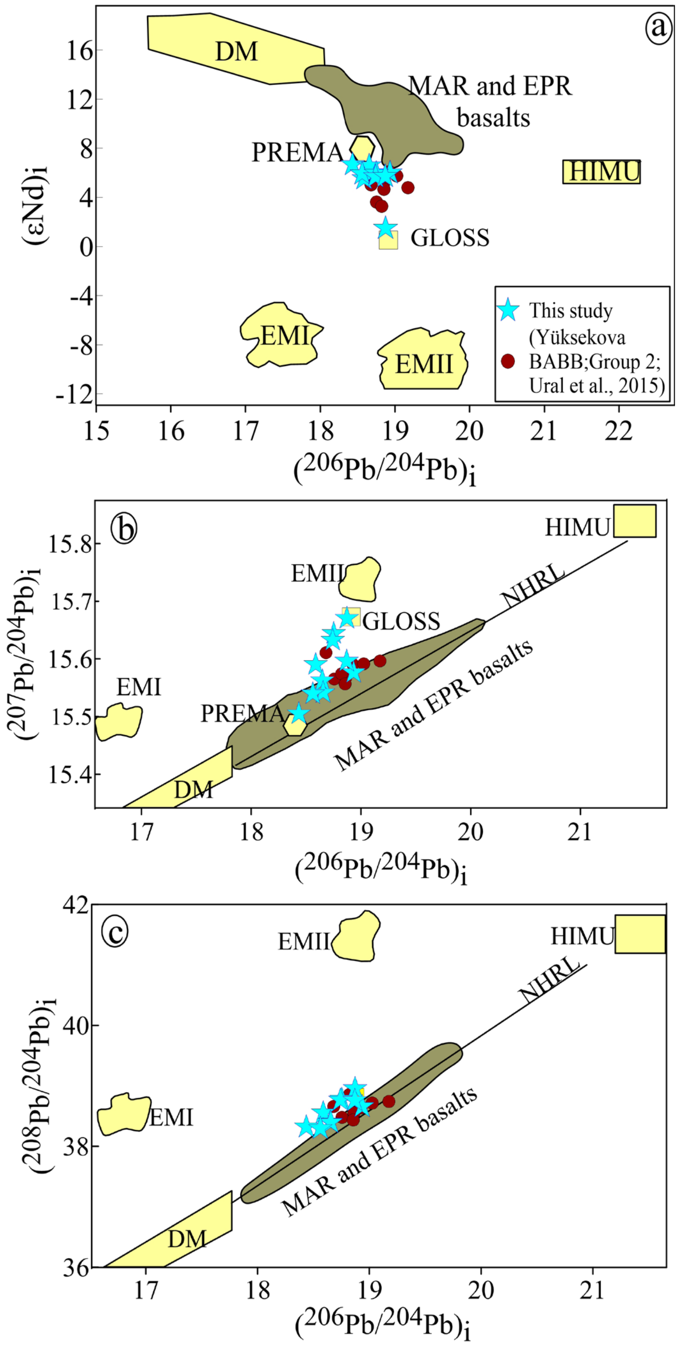

Fig. 9 - a), b), c) Age-corrected Nd and Pb isotope diagrams for the studied rocks. EMI, EMII fields are from Faure and Mensing (2005); DM, PREMA and HIMU fields are from Zindler and Hart (1986); MAR and EPR basalt values are from Hoernle et al. (2011) and Niu et al. (2002), respectively. GLOSS value is from Plank and Langmuir (1998).

Discussion

Effects of alteration

The Yüksekova volcanics display loss on ignition values (LOI) between 0.76 and 10.14 wt%, which indicates that they have experienced variable degrees of alteration. Therefore, it is essential to assess to what extent the present chemistry reflects the pristine, magmatic signatures. It is known that LILE (e.g., K, Rb, and Ba) can be easily mobilized during post-magmatic processes (i.e. weathering and metamorphism), while Th, HFSE (e.g., Zr, Nb, Ti) and REE tend to remain immobile in such conditions (e.g., Pearce 1975; Staudigel et al. 1996). To test the mobility of elements, we first use Zr-based binary plots since this element is assumed to remain highly stable under low-grade alteration (Fig. 10a-j) (e.g., Cann, 1970). These plots highlight that HFSE and REE display good correlations with Zr, attesting their immobility, whereas the scattered distribution reflected by LILE suggest their mobile nature during alteration (Fig. 10a-j). These elements also reflect some degree of correlation against LOI, which reinforce the idea that LILE were mobilized during post-magmatic processes (Fig. 10f and g).

The large range in major elements is another issue to consider (Fig. 10h-l). Based on the discussion above, K_2O is largely controlled by alteration, while TiO_2 and P_2O_5 appear to be immobile and reflect pristine values in the Yüksekova volcanics. Among the others, Si, Mg, Fe, and Ca are the elements that are known to mobilize during secondary processes. In the studied extrusives, SiO_2 and Fe_2O_3 are rather tightly clustered (when the primitive compositions are considered), and do not yield any identifiable trend. Again, no correlation vs. LOI is observed (not shown). CaO shows a very broad range for similar Zr contents, and it is highly correlated with LOI. MgO, on the other hand, is correlated with Zr, but displays scattered distribution against LOI. This suggests that CaO is heavily affected by alteration (thus it will not be used thereafter), whereas MgO appears to be relatively less affected and can be used for petrogenetic discussion. SiO_2 and Fe_2O_3 do not yield robust information in the above plots in regard to their mobility.

Fractional crystallization

The studied volcanics display compatible element concentrations lower than those of primary magmas (typically 300-500 ppm Cr, 300-400 ppm Ni, Mg# 68-76; Hess, 1992). This, therefore, suggests that they have formed from parental melt(s) through some degree of fractional crystallization, possibly involving olivine and pyroxene. Regarding the within-suite variations, MgO displays a negative correlation with SiO_2 (not shown), as expected for modification of magma with the possible removal of ferromagnesian phases. Also, Zr demonstrates a good, negative correlation with MgO (Fig. 10i), suggesting that the elemental range of Zr is somewhat controlled by fractional crystallization, and becomes concentrated in the residual liquids. Therefore, Zr can be used, to some extent, as an index of fractionation similar to MgO.

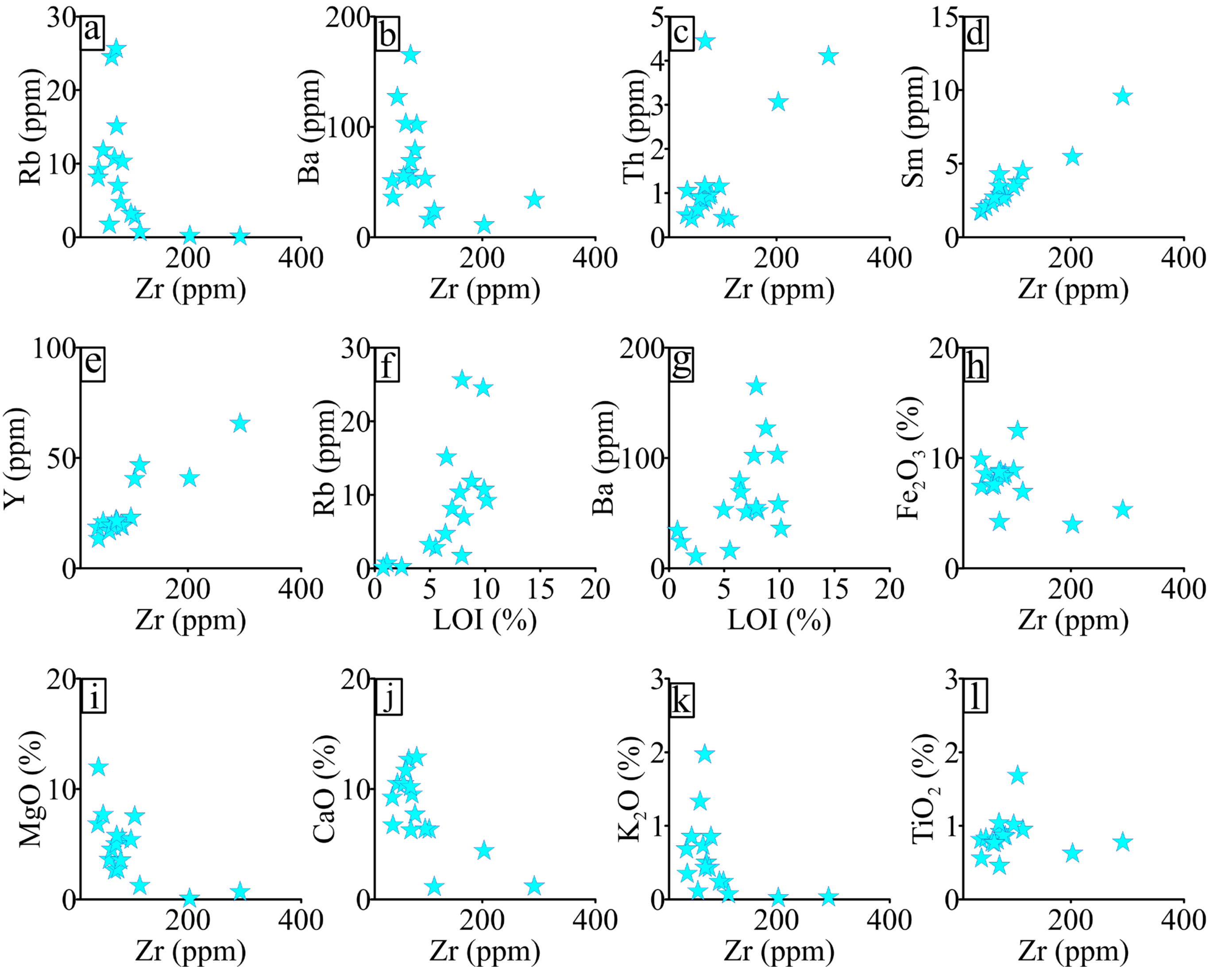

Fig. 10 - Plots of a), b), c), d), e) Zr vs. Rb, Ba, Th, Sm, Y; f), g) LOI vs. Rb, Ba; h), i), j), k) Zr vs. Fe_2O_3, MgO, CaO, K_2O, TiO_2 for the Yüksekova volcanics.

When plotted against MgO, Ni shows a broad positive correlation, which may seem somewhat scattered (Fig. 11a). However, when Ni is plotted against Zr, two issues become clear; i) Ni decreases with increasing Zr, implying the fractionation of mafic phases, particularly olivine, ii) the data define two distinct trends, which may reflect magmatic modification from at least two parental melts. In the light of this, the scattering observed in MgO is actually reduced into two trends with better correlation, supporting the olivine fractionation. The effect of mafic phases on the magmatic evolution of the volcanics is further supported by the decrease in Co and Cr at increasing Zr (Fig. 11c, d), which can be attributed to the fractionation of pyroxene. In contrast to the mafic phases, plagioclase did not participate to the fractional crystallization, as reflected by the absence of strong Eu anomalies in the REE patterns (Fig. 8b). However, the change in the slope observed in the plot of Zr vs. Al_2O_3 for the evolved compositions (for Type 2), together with mild Eu anomalies, suggest that plagioclase fractionation become dominant ain the late stages of crystallization for the Type 2 Yüksekova volcanics Fig. 11e). Fe-Ti oxides were not included in the early fractionation assemblage for the primitive compositions. However, the low Ti contents of the evolved (i.e. Si-rich) samples, as reflected by their strong negative Ti anomalies, imply a major role for the late-stage fractionation of Fe-Ti oxides (Figs. 8a, and 11). Similarly, apatite can be suggested as another late-stage fractionating phase (for the second group) based on the kink shown in the Zr-P_2O_5 plot (Fig. 11f).

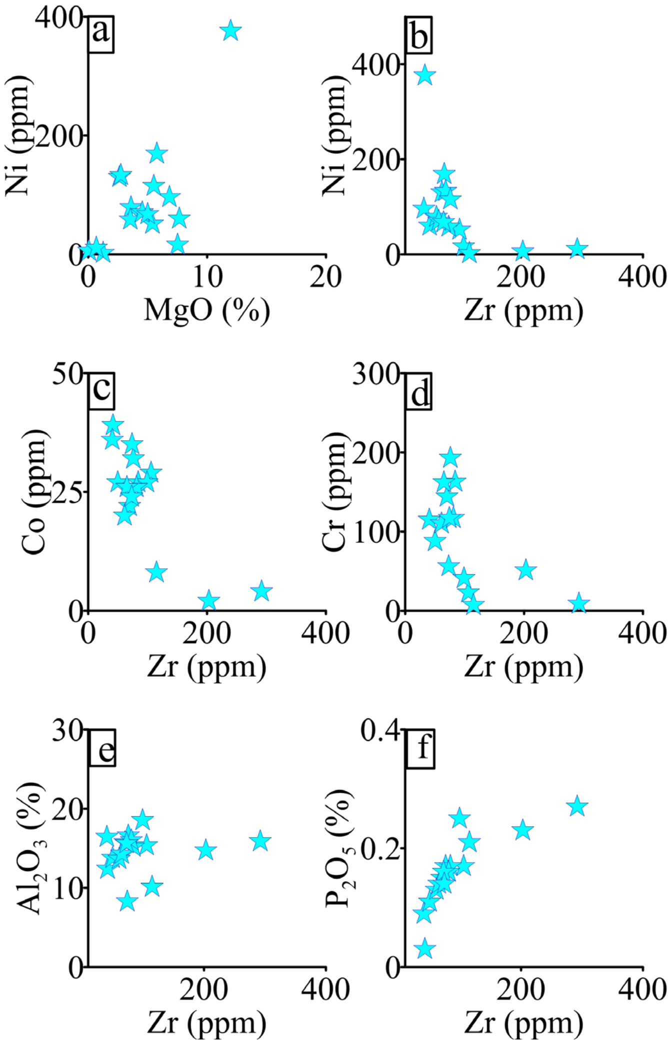

Fig. 11 - Plots of a) MgO vs. Ni; b), c), d), e), f) Zr vs. Ni, Co, Cr, Al_2O_3, P_2O_5 for the Yüksekova volcanics.

Source characteristics

To understand the mantle source characteristics, we mainly focus on the more primitive members (thus excluding the evolved samples: MDN-10, 20, 23 with 1.24, 0.06, 0.68 wt% MgO values and 73.34, 64.84, 66.21 wt% SiO_2, respectively), since it is likely that some elemental ratios can be modified during fractional crystallization. A first-order approximation to infer the nature of the mantle source can be made using absolute Nb concentrations. Based on this, the studied volcanics appear to have derived from a mantle source with enrichment levels somewhat similar or mildly enriched compared to the source of N-MORBs (Fig. 8a). This idea should be further tested using elemental ratios not affected by fractional crystallization. The immobile trace element ratios, such as Zr/Nb, and Nb/Y can be of great use to infer the source depletion/enrichment in the altered/metamorphosed igneous rocks (e.g., Sayit et al., 2020).

The depleted mantle sources (e.g., the N-MORB source) are characterized by high Zr/Nb ratios (e.g., depleted MORB mantle - DMM, Zr/Nb = 34.2; Workman and Hart, 2005), since previous melt extraction would deplete a source region in terms of more incompatible Nb (relative to Zr), thus producing an Nb-poor residual mantle. In this regard, the composition of N-MORBs potentially provides insights into the involvement of depleted mantle component. N-MORBs represent medium/high-degree melting products of the depleted mantle, therefore they potentially have Zr/Nb values close to that of the source (N-MORB Zr/Nb = 31.8; Sun and McDonough, 1989). The Zr/Nb ratios of the primitive samples vary in a broad range between 9.8 and 57.9, encompassing values both lower and higher than that of N-MORB (Fig. 12a). This suggests that the Yüksekova volcanics were possibly derived from a heterogeneous source with variable enrichment/depletion levels. This idea can also be assessed using the Nb/Y ratio (or Nb/Yb; e.g., Pearce and Peate, 1995); the lower values indicate more depleted source signatures since the higher incompatibility of Nb. The Yüksekova volcanics show a wide range of Nb/Y values between 0.07 and 0.32, supporting the hypothesis that the mantle source of these volcanics was heterogeneous. This, in turn, may suggest that the Yüksekova volcanics have tapped mantle source domains, with: i) somewhat enriched characteristics with a possible contribution from enriched components and/or low-degree melting, and ii) DMM-like characteristics, iii) previously depleted DMM-like characteristics (via melt extraction).

The elements used so far (i.e. Zr, Nb, Y, Yb) are also immobile during subduction processes (more information is given in the following paragraphs); therefore, they serve as critical indicators to understand the nature of the source before addition of subduction components. On the basis of the discussion above, the trace element evidence suggests that the Yüksekova volcanics require the involvement of a DMM-like component, whose contribution is expected to vary within the samples. The N-MORB-like samples can be envisioned to have largely tapped this source, whereas this component may have mixed with the enriched components (e.g., recycled components) to create the mildly enriched mantle sources. The samples that appear to be more depleted in terms of Zr/Nb and Nb/Y systematics, on the other hand, can be attributed to melt extraction from a DMM-like source.

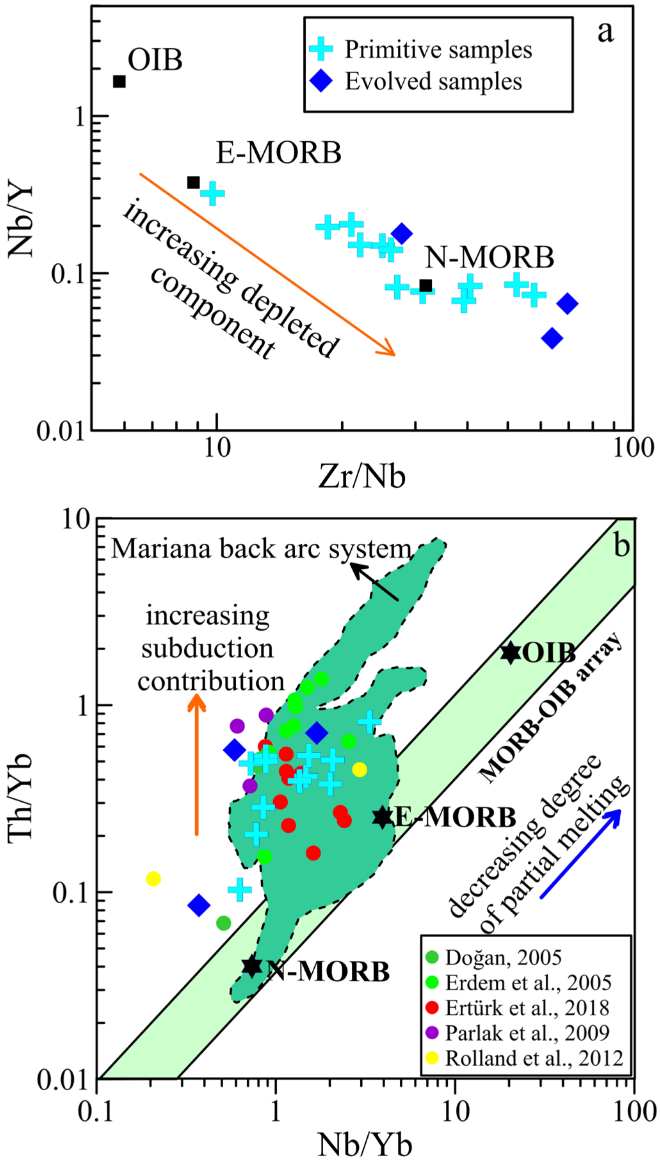

Fig. 12 - Tectonomagmatic discrimination of the Yüksekova volcanics: a) Zr/Nb vs. Nb/Y diagram; b) Nb/Yb vs. Th/Yb (Pearce and Peate, 1995). N-MORB, E-MORB, and OIB values are from Sun and McDonough (1989).

However, it must be noted that the addition of subduction component can modify the isotopic character of the source based on the extent and the nature of the material that mixes with the source (e.g., sediment melt).

The $^{143}Nd/^{144}Nd_{(i)}$ ratios of the Yüksekova volcanics are all higher than the Bulk Silicate Earth (or CHUR) with ε_{Nd} values above +5 (except for one sample with εNd = +2). Such high, positive values imply a major role for the DMM-type component in the petrogenesis of the Yüksekova volcanics, thus reinforcing the constraints obtained from the trace element systematics. However, the Nd isotopic values are not typical of DMM, which, in turn, may suggest the involvement of enriched components, such as sediments or recycled components, as mentioned earlier. The Pb isotope systematics of the volcanics are also consistent with this result. The samples display relatively enriched $^{206}Pb/^{204}Pb$ isotopic characteristics (compared to DMM), plotting on the mildly enriched/enriched portions of the Atlantic and Pacific MORB. Also, at a given $^{206}Pb/^{204}Pb$, the $^{207}Pb/^{204}Pb$ and $^{208}Pb/^{204}Pb$ ratios of the samples are elevated relative to Atlantic and Pacific MORB (Fig. 9). This issue will be further discussed in the following paragraphs.

While the Zr-Nb-Yb systematics and Nd isotopes require contribution from a depleted mantle source, some trace elements, particularly Th and La, are markedly enriched relative to Nb (Fig. 8a). This decoupled behaviour between Th-La and Nb is a common feature of the magmas from subduction-related tectonic settings (e.g., Pearce 1983). It is commonly suggested that in such environments, Nb is not mobilized by slab-derived fluids/melts but retained in the subducted slab due to Ti-rich accessory phases (e.g., rutile) (e.g., Ryerson and Watson, 1987). Thus, Nb displays strongly conservative behaviour and subsequently does not affect the elemental budget of the mantle wedge (e.g., Pearce and Peate, 1995). In contrast to Nb, Th and La are transferred from the slab to mantle wedge via fluids and sediment melts during slab dehydration and melting (e.g., Fretzdorff et al., 2002; Plank, 2005; Saccani et al., 2018). The net result of this decoupling is that the mantle wedge metasomatized by slab-derived fluids/melts is characterized by enrichment in Th and La relative to Nb, thus displaying high Th/Nb and La/Nb ratios. As noted above, such features are also shown by the Yüksekova volcanics, which may, in turn, suggest the involvement of subduction component in their mantle source. This idea can be further tested using Th-Nb-Yb systematics. The displacement from the MORB array (e.g., the Mariana arc-basin; Fig. 12b) in Nb/Yb vs. Th/Yb diagram indicates subduction-related metasomatic input. Similarly, all Yüksekova samples appear to markedly deviate from the MORB array, further supporting the role of slab-derived materials in the petrogenesis of the Yüksekova primitive melts. Another robust constraint in this regard comes from the Pb isotope systematics. Sediments are known to possess high Pb concentrations (e.g., Plank and Langmuir, 1998); thus, the addition of even a small amount of sediment would affect the Pb isotope budget of the mantle source. In the Pb isotope spaces, the Yüksekova volcanics are displaced upward from the Atlantic and Pacific MORB field and trend towards GLOSS (Fig. 9). Thus, this strongly favours the contribution of the slab-derived sediment component introduced into the mantle source of the Yüksekova volcanics during subduction. It must be noted that the two samples with the highest $^{207}Pb/^{204}Pb$ and $^{208}Pb/^{204}Pb$ may have possibly involved a significant sedimentary input. The sample with the lower ε_{Nd} (the lowest among in the dataset), combined with the high Nb/Y (the highest in the dataset), may also suggest a role for a recycled, enriched component in the petrogenesis of this sample. In summary, while Zr-Nb-Y systematics and Nd isotopes suggest an important role for the depleted mantle sources for the origin of the Yüksekova volcanics, Th-Nb-La systematics and Pb isotopes imply evidence for a subduction-related metasomatism of the source.

TECTONOMAGMATIC CONSTRAINTS

The immobile trace element systematics, which highlights the relative Th-La-enriched nature of the Yüksekova volcanics (when compared to N-MORB) (Fig. 8), suggests that these extrusives cannot have been generated at a mid-ocean ridge setting. Instead, such features can be due to the contribution from slab-derived fluids/melts, which are typical of subduction-related magmas. Therefore, the Yüksekova volcanics were most likely formed at a subduction zone involving additional input from the subducted slab, which is also evidenced particularly by the Pb isotopes.

At subduction zones, the overlying plate can be either continental or oceanic, which, in turn, may influence the geochemical nature of the produced magmas. Therefore, although the Yüksekova volcanics display subduction-related characteristics, whether the melt generation has taken place in a continental or oceanic subduction zone still needs to be constrained. The oceanic subduction zones are relatively simpler; they do not involve the continental lithosphere. Melt generation is mainly limited to the shallow asthenospheric mantle, with moderate/high degrees of melting in the spinel stability field. However, the continental lithosphere may add complexities due to the possible involvement of continental crustal materials. Besides, the enrichment of the melts can be enhanced due to deeper melting and/or enriched nature of the continental lithospheric mantle (e.g., Pearce, 1983). Therefore, it is expected that oceanic subduction zones tend to produce, in general, high Zr/Nb and low Zr/Y and Nb/Y ratios (e.g., Peate et al., 1997), whereas the opposite characteristics would characterize the continental subduction zones (e.g., Holm et al., 2014). The relatively high Zr/Nb, low Zr/Y and Nb/Y ratios of the studied volcanics are more consistent with an oceanic origin rather than continental. This hypothesis is also supported by the relatively high ε_{Nd} values of the investigated samples, which contrast with lavas from the continental subduction zones, usually showing lower or even negative ε_{Nd} values.

Additional constraints may contribute to discriminate whether the Yüksekova volcanics formed in an arc or back-arc region of an intra-oceanic subduction zone. Although arc and back-arc volcanics may show some overlap in their trace element systematics, some approximation can be made to differentiate between these two environments. Arc magmas generally acquire highly depleted characteristics (e.g., low Nb, very high Zr/Nb, low Nb/Yb), which can be attributed to (i) the melt extraction in the back-arc region, producing a highly depleted mantle transferred to the site of arc melting, and (ii) melt-extraction in the arc melting column (e.g., Woodhead al., 1993; Pearce and Peate, 1995). Compared to arc magmas, back-arc magmas are relatively more enriched, displaying generally N-MORB- or E-MORB- and OIB-type signatures in some instances (e.g., Pearce et al., 2005). Most of the Yüksekova volcanics are relatively enriched in Nb compared to N-MORB, and display high Nb/Yb ratios. This suggests that a back-arc origin can be a better alternative for the generation of the Yüksekova volcanics. This idea is also supported by the moderate Ti/V ratios, which are in contrast with the arc magmas characterized by high Ti/V values (Shervais, 1982) (Fig. 13a). A back-arc origin is also consistent with the Th-Nb systematics (Saccani, 2015; Fig. 13b).

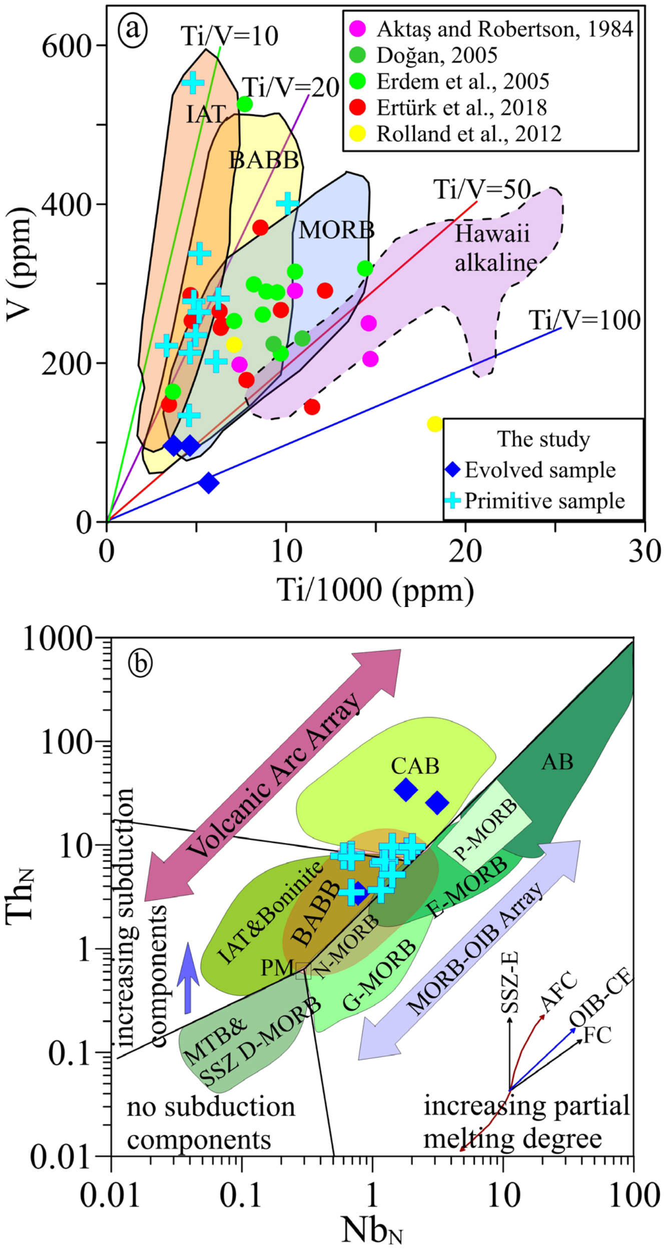

Fig. 13 - a) V-Ti/1000 (Shervais, 1982), b) Th_N vs. Nb_N (Saccani, 2015); N-MORB, E-MORB, OIB and normalization values are from Sun and McDonough (1989); Abbreviations: SSZ-E: supra-subduction zone enrichment; AFC: assimilation-fractional crystallization; OIB-CE: ocean island-type (plume-type) component enrichment; FC: fractional crystallization; MORB -mid-ocean ridge basalt; G-MORB -garnet-influenced MORB; N-MORB -normal-type MORB; E-MORB- enriched-type MORB; P-MORB -plume-type MORB; AB -alkaline ocean island basalt; IAT -low-Ti, island arc tholeiite; CAB -calc-alkaline basalt; MTB –medium Ti basalt; D-MORB -depleted-type MORB; BABB -backarc basin basalt. In both panels, Nb and Th were normalized to N-MORB composition of Sun and McDonough (1989).

GEODYNAMIC CONSTRAINTS

The geochemical characteristics of the extrusives of this study, which are mainly of basaltic composition, require the addition of slab-derived materials in their mantle sources and suggest their formation in an intra-oceanic subduction zone, possibly a back-arc setting. It is important to note that these volcanics are in primary contact with pelagic sediments, suggesting the synchronous nature of lava flows and sediments. The paleontological dating based on the radiolarians from the cherts yields Santonian-Campanian ages (Late Cretaceous), which strongly indicate that the studied basalt-chert sequences belong to the Yüksekova Complex rather than to the Maden Complex. This result is of critical importance and it is also supported by the findings of Tekin et al. (2015), which show that many outcrops in the type locality of the Maden Complex are, in fact, Late Cretaceous in age (see also Ural and Sarı, 2019).

Evidence obtained by Tekin et al. (2015) and in this study clearly show that the Maden Complex covers a smaller area than previously thought, particularly around the Maden area. Therefore, petrogenetic and geodynamic models on the origin and evolution of the Maden Complex based on the assumption that all the volcanic sequences are of Eocene age should now be reconsidered. In the geochemical studies (Aktaş and Robertson, 1984; Doğan, 2005; Erdem et al., 2005; Robertson et al., 2007; Parlak et al., 2009; Rolland et al., 2012; Ertürk et al., 2018), it appears that the so-called Maden samples show geochemical features similar to those of the Late Cretaceous Yüksekova Complex, with significant overlap in the tectonomagmatic diagrams (Figs. 7a-b, 12b, 13a). This implies that in the Maden area, where similar volcanic units with different ages are closely associated, accurate age constraints are fundamental to reveal the true identity of these units.

Based on paleontological age data, our findings in this study allow us to put some remarks on the Late Cretaceous geodynamic evolution of the region before the closure of Southern Neotethys. However, it should be noted that the Neotethys, as a whole, experienced subduction processes long before the Late Cretaceous time. The intra-oceanic subduction seems to have started in the Anisian (Middle Triassic) (Tekin et al., 2016; Sayit et al., 2017), which is later tracked towards the Late Triassic (Ma et al. 2018; Sayit et al., 2020). Then, the intra-oceanic subduction activity also continued in the Early/Middle Jurassic period. The latest stages of this activity are observed in the Cretaceous, during which a vast amount of SSZ-type products were generated. Numerous data suggest the existence of a northward-directed intra-oceanic subduction system during the Late Cretaceous in the Southern Neotethys (Sengör and Yilmaz, 1981; Yazgan, 1984; Göncüoğlu and Turhan, 1984; Parlak et al., 2009; Robertson et al., 2013). In fact, the same subduction has been also documented in the Zagros Mountains (Allahyari et al., 2010; 2014). From the late Albian onward, arc-fore arc-type magmatism started to form along this intra-oceanic subduction zone, which is marked by the Troodos, Kızildag, and Baer-Bassit ophiolites (e.g., Robertson, 2002; Karaoglan et al., 2013a; 2013b; Maffione et al., 2017). The presence of boninitic rocks in these ophiolites may imply the initial development of the subduction zone, where the boninite formation may be attributed to a highly depleted, harzburgitic mantle source. The arc magmatism continues towards the east, as evidenced by the Yüksekova volcanics. The ages of the radiolaria in the rocks intercalated with the Yüksekova volcanics suggest that oceanic arc magmatism starts at least in Albian times. In this region, the arc may have been rifted off later to give way to back-arc magmatism during Coniacian-early Maastrichtian (Ural et al., 2015; this study) (Fig. 14). Hence, a complete system of forearc (Kızıldağ ophiolites; Bağcı et al. 2005), arc and back-arc magmatism (Ural, 2012; Ural et al., 2014; 2015 and this study) was generated during the closure of the Southern Neotethys. The Southern Neotethys intra-oceanic subduction zone is further traced to the east towards Iran, whose evidence is preserved in many ophiolite bodies (e.g., Moghadam et al., 2013; Monsef et al., 2019).

The available age data suggest that Maastrichtian time designates the youngest intra-oceanic subduction-related magmatism in the Elazığ area. This period was also the time when the subduction/accretion prism material and the mélange complexes started to be emplaced towards the south onto the northern continental margin of the Arabian microplate along the Bitlis-Zagros Suture Belt. In the Elazığ area, the late Maastrichtian-Eocene interval is characterized by the lack of volcanic activity and involves a continuous deposition of flysch material, i.e., the Hazar Group, in a fault-controlled basin. These flysch deposits unconformably overlie the Yüksekova volcanics, therefore putting an upper age limit to the magmatism as pre-late Maastrichtian.

CONCLUSIONS

The Yüksekova Complex around the Maden town (SE Elazığ) dominantly consists of mafic volcanics, which are stratigraphically associated with radiolarian-bearing cherts of Santonian-Campanian age (Late Cretaceous). This implies that the volcanics cannot be related to the Maden Complex of Eocene age, which formed after the closure of the southern branch of Neotethys. The Late Cretaceous Yüksekova volcanics in the Maden region, are thus related to the Neotethys tectonic evolution. The geochemical characteristics of the extrusives suggest their formation in an intra-oceanic subduction zone, more likely at a back-arc setting. Combined with the previous data, the new evidence implies a widespread intra-oceanic subduction-related magmatism that have existed from Albian onward in the Southern Neotethys realm. In the Anatolian sector, the Yüksekova arc was rifted to give way to back-arc magmatism, representing the youngest intra-oceanic magmatism in the Elazığ area, during the Coniacian-early Maastrichtian.

ACKNOWLEDGEMENTS

This study was funded by the FÜBAP (Fırat University) MF-18.23 and MF-18.28 numbered projects. The first author is grateful to her father and brother for their supports in the field studies. The authors thank G. Borghini, E. Saccani and N.J. Bragin for their constructive comments.

REFERENCES

Açıkbaş D. and Baştuğ, C., 1975. Geology survey report and petroleum potentials of Region Cacas-Hani area northern territories. TPAO Rep., 917 (in Turkish, unpublished).

Aktaş G. and Robertson A.H.F., 1984. The Maden Complex, SE Turkey: evolution of a Neotethyan active margin, In: J.E. Dixon and A.H.F. Robertson (Eds.), The geological evolution of the Eastern Mediterranean. Geol. Soc. London Spec. Publ., 17: 375-402.

Allahyari K., Saccani E., Pourmoafi M., Beccaluva L. and Masoudi F., 2010. Petrology of mantle peridotites and intrusive mafic rocks from the Kermanshah ophiolitic complex (Zagros belt, Iran): implications for the geodynamic evolution of the Neo-Tethyan oceanic branch between Arabia and Iran. Ofioliti, 35 (2): 71-90.

Allahyari K., Saccani E., Rahimzadeh B. and Zeda O., 2014. Mineral chemistry and petrology of highly magnesian ultramafic cumulates from the Sarve-Abad (Sawlava) ophiolites (Kurdistan, NW Iran): New evidence for boninitic magmatism in intraoceanic fore-arc setting in the Neo-Tethys between Arabia and Iran. J. Asian Earth Sci., 79: 312-328.

Bağcı U., Parlak O. and Höck V., 2005. Whole-rock and mineral chemistry of cumulates from the Kızıldağ (Hatay) ophiolite (Turkey): clues for multiple magma generation during crustal accretion in the southern Neotethyan ocean. Miner. Mag., 69 (1): 53-76.

Barrett T.J. and MacLean W.H., 1997. Volcanic sequences, lithogeochemistry and hydrothermal alteration in some bimodal VMS systems. In: C.T. Barrie and M.D. Hannington (Eds.), Volcanic associated massive sulfide deposits, process and example in modern and ancient settings, Ottawa, Canada. p. 105-133.

Beken A., 1975. Geology of the Bahro area (Diyarbakır-Turkey). Master's thesis, Middle East Technical University, 39p.

Bragina L.G., 2016. Radiolarian-based zonal scheme of the Cretaceous (Albian-Santonain) of the Tethyan regions of Eurasia. Strat. Geol. Correl., 24 (2): 41-66.

Bragina L.G., Bragin N.Y., Djeric N. and Gajic V., 2014. Late Cretaceous radiolarians and age of flyschoid sediments in the Struganik Section (Western Serbia). Strat. Geol. Correl., 22 (2): 202-218.

Bragina L.G., Bragin N.Y., Kopayevich L.F., Djeric N. and Spajic N.G., 2019. Stratigraphy and microfossils (radiolarians and planktonic foraminifers) of the Upper Cretaceous (upper Santonian-lower Campanian) Struganik limestone (Western Serbia). Palaeoworld, 28: 361-380.

Cann J.R., 1970. Rb, Sr, Y, Zr and Nb in some ocean floor basaltic rocks. Earth Planet. Sci. Lett., 10: 7-11.

Dewey J.F., Pitman W.C., Ryan W.B.F. and Bonnin J., 1973. Plate tectonics and evolution of Alpine system. Geol. Soc. Am. Bull., 84: 3137-3180.

Doğan Ş., 2005. Petrography and petrology of metaophiolites in the vicinity Kömürhan Bridge (Elazığ-Malatya), Fırat Univ.y, Graduate School Sci. Techn., Master Thesis, 59 pp. (in Turkish, with English abstract).

Erdem E., Beyarslan M. and Kılıç D., 2005. Petrographic and petrological characteristics of the volcanics of the Maden Complex. Geosound, 46: 107-123.

Erdoğan B., 1982. Geology and volcanic rocks of the Southeast Anatolian ophiolite belt of the Ergani-Maden region. Bull Geol Soc Turk., 25: 49-59 (in Turkish with English abstract).

Erler A., 1983. Tectonic setting of the massive sulphide deposit of the Southeast Anatolian thrust belt. In: O. Tekeli and M.C. Göncüoğlu (Eds.). Geology of the Taurus Belt. General Director Miner. Res. Expl. (MTA), Ankara, p. 309-316.

Ertürk M.A., Beyarslan M. and Chung S.L. T.H., 2018. Eocene magmatism (Maden Complex) in the Southeast Anatolian orogenic belt: Magma genesis and tectonic implications. Geosci. Front., 9 (6): 1829-1847.

Faure G. and Mensing T.M., 2005. Isotopes: Principles and applications, 3rd ed., John Wiley and Sons, USA, 897 pp.

Foreman H.P., 1971. Cretaceous radiolaria, Leg 7. DSDP. In: E.L. Winterer, W.R. Riedel et al. (Eds.), Init. Rep. DSDP, Washington D.C., 7: 1673-1693.

Foreman H.P., 1973a. Radiolaria of Leg 10 with systematic and ranges for the families Amphyndacidae, Artostrobidae, Theoperidae. Init. Rep. DSDP, Washington D.C., 10: 407-474.

Foreman H.P., 1973b. Radiolaria from DSDP Leg 20. In: B.C. Heezen, J.D.Mac Gregor et al. (Eds.), Init. Rep. DSDP, Washington D. C., 20: 249-305.

Foreman H.P., 1975. Radiolaria from the North Pacific, DSDP, Leg, 32. In: R.L Larson et al. (Eds.), Init. Rep. DSDP covering leg 32 of the crises of the drilling vessel Glomar Challenger, Washington, D.C., 32: 579-676.

Fretzdorff S., Livermore R.A., Devey C.W., Leat P.T. and Stoffers P., 2002. Petrogenesis of the back arc East Scotia Ridge, south Atlantic Ocean: J. Petrol., 43: 1435-1467.

Galer S.J.G. and Abouchami W., 1998. Practical application of lead triple spiking for correction of instrumental mass discrimination. Miner. Mag., 62: 491-492.

Göncüoğlu M.C., 2019. A Review of the Geology and Geodynamic Evolution of Tectonic Terranes in Turkey. In: Pirajno F., Ünlü T., Dönmez C., Şahin M. (eds) Mineral Resources of Turkey. Modern Approaches in Solid Earth Sciences, 16. Springer, Cham. https://doi.org/10.1007/978-3-030-02950-0_2.

Göncüoğlu M.C. and Turhan N., 1984. Geology of the Bitlis Metamorphic Belt. In: O. Tekeli, and M.C. Göncüoğlu (Eds). The geology of the Taurus Belt. Int Symp Proceed., MTA, Ankara, p. 237-244.

Göncüoğlu M.C., Dirik K. and Kozlu H., 1997. General characteristics of pre-Alpine and Alpine Terranes in Turkey: Explanatory notes to the terrane map of Turkey: Ann. Géol. Pays Hellén., 37: 515-536.

Hempton M.R., 1984. Results of detailed mapping near lake Hazar Eastern Taurus mountains. In: O. Tekeli and M.C. Göncüoğlu (Eds.). The geology of the Taurus Belt. Int Symp Proc, MTA, Ankara, p. 223-228.

Hempton M.R., 1985. Structure and deformation history of the Bitlis suture near Lake Hazar, SE Turkey. Geol Soc Am Bull., 96: 223-243.

Hempton M.R. and Savcı G., 1982. Petrological and structural features of Elazığ volcanic complex. Geol. Bull. Turk., 25 (2): 143-151.

Herece E., Akay E., Kücümen Ö. and Sariaslan M., 1992. Geology of Elazığ-Sivrice and Palu region. General Direct. Miner. Res. Expl. (MTA) Rep. 9634, 108 pp. (In Turkish, unpublished).

Hess, P.C., 1992. Phase equilibria constraints on the origin of ocean floor basalts. Geophys. Monogr., 71: 67-102.

Hoernle K., Hauff F., Kokfelt T.F., Haase K., Garbe-Schönberg D. and Werner R., 2011. On- and off-axis chemical heterogeneities along the South Atlantic Mid-Ocean-Ridge (5-11°S): Shallow or deep recycling of ocean crust and/or intraplate volcanism?. Earth Planet. Sci. Lett., 306: 86-97.

Holm P.M., Søager N., Dyhr C.T. and Nielsen M.R., 2014. Enrichments of the mantle sources beneath the Southern Volcanic Zone (Andes) by fluids and melts derived from abraded upper continental crust. Contrib. Miner. Petrol., 167: 1004.

İleri S., Salancı B., Bitem M. and Doğan R. 1976. Ergani-Maden copper deposit and plate tectonics: Bull. Geol Soc. Turk., 19: 133-142.

Karaoğlan F., Parlak O., Klotzli U., Koller F. and Rızaoğlu T., 2013a. Age and duration of intra-oceanic arc volcanism built on a suprasubduction zone type oceanic crust in southern Neotethys, SE Anatolia: Geosci. Front., 4 (4): 399-408.

Karaoğlan F., Parlak O., Klötzli U., Thöni M. and Koller F., 2013b. U-Pb and Sm-Nd geochronology of the ophiolites from the SE Turkey: implications for the Neotethyan evolution. Geodyn. Acta, 25 (3-4): 146-161.

Ketin İ., 1948. Ergani-Eğil Bölgesinin jeolojik etüdü: MTA Derleme No: 2015.

Khoklova I.E., Bragina L.G and Krasheninnikov V.A., 1994. Zonal stratigraphy of the Upper Cretaceous and Paleogene deposits of the Key Perapedhi section (southern Cyprus) by means of radiolarians and correlation with the foreminiferal zones. In: V.A. Krashininokov and J.K. Hall (Eds.), Geological structure of the northwestern Mediterranean (Cruise 5 of the Research Vessel Akademik Nikolaj Strakhov). Jaruselam, p. 219-250.

Korchagin O.A., Bragina L.G. and Bragin N.Y., 2012. Planktonic foraminifers and radiolarians from the Coniacian-Santonian deposits of the Mt. Ak-Kaya, Crimean Mountains, Ukraine. Stratigr. Geol. Correl., 20 (1): 73-96.

Kılıç A.D., 2009. Petrographical and geochemical properties of plagiogranites and gabbros in Guleman ophiolite. Bull. Miner. Res. Expl., 139: 33-49.

Köküm M. and İnceöz M., 2018. Structural analysis of the northern part of the East Anatolian Fault System. J. Struct. Geol., 114: 55-63.

Köküm M. and İnceöz M., 2020. Paleostress analysis of the Yeşilyurt-Elazığ Fault Zone and its importance for the tectonic evolution, East Turkey. J. Struct. Geol., 138: 104093.

Ma X., Meert J.G., Xu Z. and Yi Z., 2018. Late Triassic intra-oceanic arc system within Neotethys: Evidence from cumulate appinite in the Gangdese belt, southern Tibet. Lithosphere, 10: 545-565.

Maffione M., van Hinsbergen D.J., de Gelder G.I., van der Goes F.C. and Morris A., 2017. Kinematics of Late Cretaceous subduction initiation in the Neo-Tethys Ocean reconstructed from ophiolites of Turkey, Cyprus, and Syria. J. Geophys. Res., Solid Earth, 122 (5): 3953-3976.

Michard A., Yazidi A., Benziane F., Hollard H. and Willefert S., 1982. Foreland thrusts and olistromes on the pre-Sahara margin of the Variscan orogen, Morocco. Geology, 10 (5): 253-256.

Michard A., Whitechurch H., Ricou L.E., Montigny R. and Yazgan E., 1985. Tauric subduction (Malatya-Elazığ province) and its bearing on the tectonics of the Tethyan realm in Turkey. In: J.E. Dixon and A.H.F. Robertson (Eds.), The geological evolution of the eastern Mediterranean. Geol. Soc. London Spec. Publ., 17: 361-373.

Moghadam H.S. Whitechurch H., Rahgoshay M. and Monsef I., 2009. Significance of Nain-Baft ophiolitic belt (Iran): Short-lived, transtensional Cretaceous back-arc oceanic basins over the Tethyan subduction zone. C.R. Geosci., 341 (12): 1016-1028.

Moghadam H.S., Mosaddegh H. and Santosh M., 2013. Geochemistry and petrogenesis of the Late Cretaceous Haji-Abad ophiolite (Outer Zagros Ophiolite Belt, Iran): implications for geodynamics of the Bitlis-Zagros suture zone. Geol. J., 48 (6): 579-602.

Monsef I., Rahgoshay M., Pirouz M., Chiaradia M., Grégoire M. and Ceuleneer G., 2019. The Eastern Makran Ophiolite (SE Iran): evidence for a Late Cretaceous fore-arc oceanic crust. Int. Geol. Rev., 61: 1313-1339.

M.T.A., 2002. Geological Map of Turkey of 1:500.000 scale, the Erzurum Quad-rangale, Gen. Direct. Miner. Res. Expl., (MTA), Ankara, Turkey.

M.T.A., 2011. 1/100.000 ölçekli Türkiye Jeoloji Haritası, Maden Tetkik ve Arama Genel Müdürlüğü, Ankara (in Turkish).

Nakaseko K. and Nishimura A., 1981. Upper Jurassic and Cretaceous Radiolaria from the Shimato Group in Southwest Japan. Sci. Rep, Col. Gen. Educ., Osaka Univ. 30 (2): 133-203.

Nakaseko K., Nishumara A. and Sugano K., 1979. Cretaceous radiolaria in the Shimanto Belt, Japan. News Osaka Micropal., Spec. Vol., 2: 1-49.

Niu Y., Regelous M., Wendt I.J., Batiza R. and O'Hara M.J., 2002. Geochemistry of near-EPR seamounts: importance of source vs. process and the origin of enriched mantle component. Earth Planet. Sci. Lett., 199: 327-345.

O'Dogherty L., 1994. Biochronology and paleontology of Mid-Cretaceous radiolarians from Northern Apennines (Italy) and Betic Cordillera (Spain). Mém. Géol. (Lausanne), 21: 415 pp.

Özçelik M., 1985. Geology of the Maden magmatic rocks and a geochemical approach to their tectonic settings, southeast Malatya. Geol. Bull. Turk., 28: 19-34.

Özdemir Y., 2016. Geochemistry of tholeiitic to alkaline lavas from the east of Lake Van (Turkey): Implications for a late Cretaceous mature supra-subduction zone environment. J. Afr. Earth Sci., 120: 77-88.

Özkan Y.Z., 1983. A geochemical approach to the origin problem of Caferi Volcanics. In: Proceed. Chamber of the Geol. Engin. Ann. Meet.. Bull. Geol. Congr. Turk., Ankara, 4: 53-58.

Özkaya I., 1978. Stratigraphy of Ergani-Maden vicinity. Geol. Bull. Turk., 21: 129-139.

Parlak O., Rizaoğlu T., Bagci U., Karaoglan F. and Höck V., 2009. Tectonic significance of the geochemistry and petrology of ophiolites in southeast Anatolia, Turkey. Tectonophysics, 473: 173-187.

Pearce J.A., 1975. Basalt geochemistry used to investigate past tectonic environments on Cyprus. Tectonophysics, 25 (1-2): 41-67.

Pearce J.A., 1983. Role of the sub-continental lithosphere in magma genesis at active continental margins. In: C.J. Hawkesworth and M.J. Norry (Eds.), Continental basalts and mantle xenoliths. Shiva Cheshire, UK, p. 230-249.

Pearce J.A., 1996. A users's guide to basalt discrimination diagrams, In: D.A. Wyman (Ed.), Trace element geochemistry of volcanic rocks. Applications for massive sulphide exploration. Geol. Ass. Can., Short Course Notes, 12: 79-113.

Pearce J.A. and Peate D.W., 1995. Tectonic implications of the composition of volcanic arc magmas. Ann. Rev. Earth Planet. Sci, 23: 251-286.

Pearce J.A., Stern R.J., Bloomer S.H. and Fryer P., 2005. Geochemical mapping of the Mariana arc-basin system: Implications for the nature and distribution of subduction components. Geochem. Geophys. Geosyst., 6 (7).

Peate D.W., Pearce J.A., Hawkesworth C.J., Colley H., Edwards C.M. and Hirose K., 1997. Geochemical variations in Vanuatu arc lavas: the role of subducted material and a variable mantle wedge composition. J. Petrol., 38 (10): 1331-1358.

Perincek D., 1979. The geology of Hazro-Korudag-Cüngüs-Maden-Ergani-Hazar-Elazığ-Malatya Area. Guide Book, Geol. Bull. Turk., 33 pp.

Perincek D., 1980. Effects on the sediment on the tectonic evolution of in north of the Arabian continent. Proceed. 5th Petrol. Congr of Turkey, Ankara, p. 77-93 (in Turkish).

Perinçek D., 1990. Stratigraphy of the Hakkari province, Southeast Turkey. TAPG Bull., 2 (1): 21-68 (in Turkish with English abstract).

Perincek D. and Özkaya, I., 1981. Tectonic evolution of the northern margin of Arabian plate. Bull. Inst. Earth Sci. Hacettepe Univ., 8: 91-101.

Plank T., 2005. Constraints from thorium/lanthanum on sediment recycling at subduction zones and the evolution of the continents. J. Petrol., 46 (5): 921-944.

Plank T. and Langmuir C.H., 1998. The chemical composition of subducting sediment and its consequences for the crust and mantle. Chem. Geol., 145 (3-4): 325-394.

Riedel W.R. and Sanfilippo A., 1974. Radiolaria from the southern Indian Ocean, DSDP Leg 26. In: T.A. Davis, B.P. Luyendyke et al. (Eds.), Init. Rep. DSDP., Washington, 26: 771-783.

Rigo de Righi M.R. and Cortesini A., 1964. Gravity tectonics in Foot Hills Structure belt of Southeast Turkey. AAPG, 48: 1911-1937.

Rizaoğlu T., Parlak O., Höck V. and İsler F., 2006. Nature and significance of Late Cretaceous ophiolitic rocks and its relation to the Baskil granitoid in Elazığ region, SE Turkey. Geol. Soc. London Spec. Publ., 260: 327-350.

Rizaoğlu T., Parlak O., Höck V., Koller F., Hames W.E. and Billor Z., 2009. Andean type active margin formation in the Eastern Taurides. Geochemical and geochronological evidence from the Baskil Granitoid, SE Turkey. Tectonophysics, 473: 188-207.

Rizeli M.E., Beyarslan M., Wang K.L. and Bingöl A.F., 2016. Mineral chemistry and petrology of mantle peridotites from the Guleman ophiolite (SE Anatolia, Turkey): Evidence of a forearc setting. J. Afr. Earth Sci., 123: 392-402.

Robertson A.H.F., 2002. Overview of the genesis and emplacement of Mesozoic ophiolites in the Eastern Mediterranean Tethyan region. Lithos, 65: 1-67.

Robertson A.H.F., Parlak O., Rızaoğlu T., Ünlügenç U.C., İnan N., Taslı K. and Ustaömer T., 2007. Tectonic evolution of the South Tethyan Ocean: evidence from the Eastern Taurus mountains (Elazığ region, SE Turkey). In: A.C. Ries, R.W.H. Butler and R.H. Graham (Eds.)., Deformation of the continental crust. The legacy of Mike Coward. Geol. Soc. London Spec. Publ., 272: 231-270.

Robertson A.H.F., Parlak O. and Ustaömer T., 2013. Late Palaeozoic-Early Cenozoic tectonic development of Southern Turkey and the easternmost Mediterranean region: evidence from the interrelations of continental and oceanic units. Geol. Soc. London Spec. Publ., 372 (1): 9-48.

Rolland Y., Perinçek D., Kaymakçı N., Sosson M., Barrier E. and Avagyan A., 2012. Evidence for ~ 80-75 Ma subduction jump during Anatolide-Tauride-Armenian block accretion and ~ 48 Ma Arabia-Eurasia collision in Lesser Caucasus-East Anatolia. J. Geodyn., 56: 76-85.

Rolland Y., Hässig M., Bosch D., Bruguier O., Melis R., Galoyan G., Topuz G., Sahakyan L., Avagyan A. and Sosson M., 2020. The East Anatolia-Lesser Caucasus ophiolite: An exceptional case of large-scale obduction, synthesis of data and numerical modelling. Geosci. Front., 11 (1): 83-108.

Ross P.S. and Bedard J.H., 2009. Magmatic affinity of modern and ancient subalkaline volcanic rocks determined from trace-element discriminant diagrams. Can. J. Earth Sci., 46: 823-839.

Ryerson F.J. and Watson E.B., 1987. Rutile saturation in magmas: implications for Ti-Nb-Ta depletion in island-arc basalts. Earth Planet. Sci. Lett., 86 (2-4): 225-239.

Saccani E., 2015. A new method of discriminating different types of post-Archean ophiolitic basalts and their tectonic significance using Th-Nb and Ce-Dy-Yb systematics. Geosci. Front., 6 (4): 481-501.

Saccani E., Dilek Y. and Photiades A., 2018. Time-progressive mantle-melt evolution and magma production in a Tethyan marginal sea: A case study of the Albanide-Hellenide ophiolites. Lithosphere, 10 (1): 35-53.

Sanfilippo A. and Riedel W. R., 1985. Cretaceous Radiolaria. In: H.M. Bollli, J.B. Saunders and K. Perch-Nielson (Eds.), Plankton stratigraphy, Cambridge Univ. Press, p. 573-630.

Sar A., Ertürk M.A. and Rizeli M.E., 2019. Genesis of Late Cretaceous intra-oceanic arc intrusions in the Pertek area of Tunceli Province, eastern Turkey, and implications for the geodynamic evolution of the southern Neo-Tethys: Results of zircon U-Pb geochronology and geochemical and Sr-Nd isotopic analyses. Lithos, 350-351, 105263.

Sayit K., Bedi Y., Tekin U.K., Göncüoğlu M.C. and Okuyucu C., 2017. Middle Triassic back-arc basalts from the blocks in the Mersin Mélange, southern Turkey: Implications for the geodynamic evolution of the Northern Neotethys. Lithos, 268: 102-113.

Sayit K., Bedi Y., Tekin U.K. and Okuyucu C., 2020. Carnian (Upper Triassic) lavas and tuffites from the Mersin Mélange: Evidence for ıntraoceanic arc rifting in the Northern Neotethys. J. Geol., 128 (5): 445-464.

Sengör A.M.C. and Yilmaz Y., 1981. Tethyan evolution of Turkey: A plate tectonic approach. Tectonophysics, 75: 181-241.

Shervais J.W., 1982. Ti-V plots and the petrogenesis of modern and ophiolitic lavas. Earth Planet. Sci. Lett., 59: 101-118.

Squinabol S., 1903. Le Radiolarie dei noduli selciosi nella Scaglia degli Euganei. Riv. It. Pal., 9: 105-150.

Soycan H. and Hakyemez A., 2018. The first calibration of radiolarian biochronology with Late Cretaceous (latest Coniacian-Santonian-early Campanian) planktonic foraminifera in the volcano-sedimentary sequences of the eastern Pontides, NE Turkey. Cret. Res., 85: 319-348.

Staudigel H., Plank T., White B. and Schmincke H.U., 1996. Geochemical fluxes during seafloor alteration of the basaltic upper oceanic crust: DSPS sites 417 and 418. Geophys Monogr., 96: 19-38.

Sun S.S. and McDonough W.F., 1989. Chemical and isotopic systematics of oceanic basalts; implications for mantle composition and processes. In: A.D. Saunders and M.J. Norry (Eds.), Magmatism in the ocean basins. Geol. Soc. London Spec. Publ., 42: 313-345.

Sungurlu O., 1974. Geology of the northern part of VI. District. 2nd Petroleum Congr of Turkey, Turk. Ass. Petrol. Geol., p. 85-107 (in Turkish with English abstract).

Tekin U.K., Ural M., Göncüoğlu M.C., Arslan M. and Kürüm S., 2015. Upper Cretaceous radiolarian ages from an arc-back-arc within the Yüksekova Complex in the southern Neotethys mélange, SE Turk. C. R. Palevol, 14: 73-84.

Tekin U.K., Bedi Y., Okuyucu C., Göncüoğlu M.C. and Sayit K., 2016. Radiolarian biochronology of upper Anisian to upper Ladinian (Middle Triassic) blocks and tectonic slices of volcano-sedimentary successions in the Mersin Mélange, southern Turkey: New insights for the evolution of Neotethys. J. Afr. Earth Sci., 124: 409-426.

Ural M., 2012. Petrochemistry, petrology and age of the basic volcanites of the Yüksekova Complex around Elazığ and Malatya. Fırat Univ., Graduate School of Sci.. Techn., Ph.D Thesis, 174 pp. (in Turkish, with English abstract).

Ural M. and Kaya Sari M., 2019. Paleogeographic and age findings on planktonic foraminiferal assemblages of Yüksekova Complex in the Northeast of Elazığ (Eastern Turkey). IOP Conf. Series: Earth Environ. Sci., 362 (1), p. 012146.

Ural M. and Kürüm S., 2009. Microscopic and diffractometric studies ınferred from Skarn Zonations between the Keban Metamorphites and Elazığ Magmatites, around Elazığ. Turk. J. Sci. Techn., 4 (2).

Ural, M. and Sari B., 2019. New planktonic foraminifera data from the Upper Cretaceous pelagic limestones of the Yüksekova Complex in the Maden area (Southeast of Elazığ, Eastern Turkey). IOP Conference Series, Earth Environ. Sci., 362 (1), p. 012121.

Ural M., Göncüoğlu M.C., Arslan M., Tekin U.K. and Kürüm S., 2014. Petrological and paleontological evidence for generation of a arc-back arc system within the closing southern branch of Neotethys during the Late Cretaceous. In: A. Begiraj et al. (Eds.), Proceed. 20th CBGA Congr., Bull. Shk. Gjeol., Spec. Iss., 2/2014: 51-54.

Ural M., Arslan M., Göncüoğlu M.C., Tekin U.K. and Kürüm S., 2015. Late Cretaceous arc and back-arc formation within the Southern Neotethys: whole-rock, trace element and Sr-Nd-Pb isotopic data from basaltic rocks of the Yüksekova Complex (Malatya-Elazığ, SE Turkey). Ofioliti, 40 (1): 53-72.

Ural M., Sayit K., Koralay O.E. and Göncüoğlu M.C., 2021. Geochemistry and Zircon U-Pb dates of Felsic-Intermediate Members of the Late Cretaceous Yüksekova Arc Basin: Constraints on the evolution of the Bitlis-Zagros Branch of Neotethys (Elazığ, E Turkey). Acta Geol. Sinica - English Ed., 95 (4): 1199-1216.

Uysal I., Kapsiotis A., Akmaz R.M., Saka S. and Seitz H.M., 2018. The Guleman ophiolitic chromitites (SE Turkey) and their link to a compositionally evolving mantle source during subduction initiation. Ore Geol. Rev., 93: 98-113.

Winchester J. and Floyd P.A., 1977. Geochemical discrimination of different magma series and their differentiation products using immobile elements. Chem. Geol., 20: 325-43.

Woodhead J., Eggins S. and Gamle J., 1993. High field strenght and transition element systematics in island arc and back-arc basin basalts: evidence for multi-phase melt extraction and a depleted mantle wedge. Earth Planet. Sci. Lett., 114: 491-504.

Workman R.K. and Hart S.R., 2005. Major and trace element composition of the depleted MORB mantle (DMM). Earth Planet. Sci. Lett., 231 (1-2): 53-72.

Yamauchi M., 1982. Upper Cretaceous radiolarians from the Northern Shimanto Belt along the course of Sihamanto River, Kochi Prefacture, Japan. News Osaka Micropal. Spec. Vol., 5: 383-397.

Yazgan E., 1981. A study of active continental paleomargin in the eastern Taurides (Upper Cretaceous-Middle Eocene) Malatya-Elazığ (eastern Turkey). Bull Inst Earth Sci Hacettepe Univ., 7: 83-104. (in Turkish, with English abstract).

Yazgan E., 1983. A Geotraverse between the Arabian platform and the Munzur nappes, In: Guide Book for excursion V. Int Symp on Geology of the Taurus Belt, MTA, Ankara, p. 1-17.

Yazgan E., 1984. Geodynamic evolution of the Eastern Taurus Region (Malatya-Elazığ area, Turkey). In: O. Tekeli and M.C. Göncüoglu (Eds.), Int. Symp. Geology of the Taurus Belt. Proceed., MTA, Ankara, p. 199-208.

Yazgan E., 1987. Malatya Güneydogusunun jeolojisi ve Dogu Toroslann jeodinamik evrimi. MTA, Geol. Dept. Rrt, Arch., 8272, Ankara (unpubl. in Turkish).

Yazgan E. and Chessex R., 1991. Geology and tectonic evolution of the southestern Taurides in the region of Malatya. T.P.J.D. Bull., 3 (1): 1-42.

Yazgan E., Michard A., Whitechurch H. and Montigny R., 1983. Le Taurus de Malatya (Turquie orientale), élément de la suture sud-téthysienne. Bull. Soc. Géol. Fr., 25 (1): 59-69.

Yıldırım E., 2015. Geochemistry, petrography and tectonic significance of the ophiolitic rocks, felsic intrusions and Eocene volcanic rocks of an imbrication zone (Helete area, Southeast Turkey). J. Afr. Earth Sci., 107: 89-107.

Yilmaz Y., 1993. New evidence and model on evolution of Southeast Anatolian orogen. Geol. Soc. Am. Bull.,105: 251-271.

Yilmaz Y. and Yiğitbaş E., 1991. The different ophiolitic-metamorphic assemblages of the SE Anatolia and their significance in the geological evolution of the region. Proceed. 8th Petrol. Congr. Turkey, p. 128-140 (in Turkish with English abstract).

Yigitbas E. and Yilmaz Y., 1996. Post-Late Cretaceous strike-slip tectonics and its implications for the Southeast Anatolian orogen, Turkey. Int. Geol. Rev., 38 (9): 818-831.

Yilmaz Y., Yigitbas E. and Genc S., 1993. Ophiolitic and metamorphic assemblages of southeast Anatolia and their significance in the geological evolution of the orogenic belt. Tectonics, 12 (5): 1280-1297.

Zindler A. and Hart S., 1986. Chemical geodynamics. Ann. Rev. Earth Planet. Sci., 14 (1): 493-571.

Received, August 28, 2021
Accepted, December 5, 2021